

## High interannual surface $p\text{CO}_2$ variability in the Southern Canadian Arctic Archipelago's Kitikmeot Sea.

Richard P. Sims<sup>1</sup>, Mohamed M M Ahmed<sup>1,2,3</sup>, Brian J. Butterworth<sup>4,5</sup>, Patrick J. Duke<sup>6</sup>, Stephen F. Gonski<sup>7</sup>, Samantha F. Jones<sup>1</sup>, Kristina A. Brown<sup>8,9</sup>, Christopher J. Mundy<sup>9</sup>, William J. Williams<sup>8</sup>, Brent G. T. Else<sup>1</sup>,

<sup>1</sup>Department of Geography, University of Calgary, Calgary, Alberta, T2N 1N4, Canada

<sup>2</sup>Geology Department, Beni-Suef University, 101 Salah Salem St., Bani Sweif, 62511, Egypt

<sup>3</sup>Education and Research Group, Esri Canada, Calgary, Alberta, T2P 3T7, Canada

<sup>4</sup>Cooperative Institute for Research in Environmental Sciences, University of Colorado, Boulder, Colorado, USA

<sup>5</sup>NOAA Physical Sciences Laboratory, Boulder, Colorado, USA

<sup>6</sup>School of Earth and Ocean Sciences, University of Victoria, Victoria, British Columbia, Canada

<sup>7</sup>School of Marine Science and Policy, University of Delaware, Lewes, Delaware, USA

<sup>8</sup>Institute of Ocean Sciences, Fisheries and Oceans Canada, Sidney, British Columbia, Canada

<sup>9</sup>Centre for Earth Observation Science, Department of Environment and Geography, University of Manitoba, Winnipeg, MB R3T 2N2, Canada

Correspondence to: Richard P. Sims (richardpeter.sims@ucalgary.ca)

**Abstract.** Warming of the Arctic due to climate change means the Arctic Ocean is now ice-free for longer, as sea ice melts earlier and refreezes later. Yet, it remains unclear how the extended ice-free period will impact carbon dioxide ( $\text{CO}_2$ ) fluxes due to scarcity of surface ocean  $\text{CO}_2$  measurements. Baseline measurements are urgently needed to understand spatial and temporal air-sea  $\text{CO}_2$  flux variability in how air-sea  $\text{CO}_2$  fluxes will spatially and temporally vary in a changing Arctic Ocean. There is also uncertainty as to whether the previous basin-wide surveys are representative of the many smaller bays and inlets that make up the Canadian Arctic Archipelago (CAA). By using a research vessel that is based in the remote Inuit community of Ikaluqtuutik Cambridge Bay (Cambridge Bay Ikaluqtuutik, Nunavut), we have been able to reliably survey  $p\text{CO}_2$  shortly after ice melt and access previously unsampled bays and inlets in the nearby region. Here we present four years of consecutive summertime  $p\text{CO}_2$  measurements collected in the Kitikmeot Sea in the southern Canadian Arctic Archipelago CAA. Overall, we found that this region is a sink for atmospheric  $\text{CO}_2$  in August (average of all calculated fluxes over the four cruises was  $-4.64$ – $-8.3$   $\text{mmol m}^{-2} \text{d}^{-1}$ ) but the magnitude of this sink varies substantially between years and locations (average calculated fluxes of  $+3.58$ – $0.41$ ,  $-2.96$ – $-7.70$ ,  $-16.79$ – $-21.26$  and  $-0.57$ – $-2.08$   $\text{mmol m}^{-2} \text{d}^{-1}$  during the 2016, 2017, 2018 and 2019 cruises, respectively). Surface ocean  $p\text{CO}_2$  varied by up to  $442$ – $156$   $\mu\text{atm}$  between years; this highlights the importance of repeat observations in the Arctic region, as this high interannual variability would not have been captured by sparse and infrequent measurements. We find that the surface ocean  $p\text{CO}_2$  value of the surface ocean at the time of ice melt is extremely important in constraining the magnitude of the air-sea  $\text{CO}_2$  flux throughout the ice-free season. However, further constraining the air-sea  $\text{CO}_2$  flux in the Kitikmeot Sea will require a better understanding of how  $p\text{CO}_2$  changes outside of the summer season. Surface ocean  $p\text{CO}_2$  measurements made in the small bays and inlets of the Kitikmeot Sea were  $\sim 20$ – $40$   $\mu\text{atm}$  lower than in the main channels, and, surface ocean  $p\text{CO}_2$  measurements made close in

[time](#) to ice breakup (i.e., within 2 weeks) were  $\sim 50$ – $100$   $\mu\text{atm}$  lower than measurements made  $>4$  weeks after breakup. As [previous](#) basin-wide surveys of the CAA have focused on the deeper shipping channels and rarely measure close to the ice break-up date, we hypothesize that there may be an observational bias in previous studies, leading to an underestimate of the  $\text{CO}_2$  sink in the [Canadian Arctic Archipelago](#) CAA. These high-resolution measurements constitute an important new baseline for gaining a better understanding of the role this region plays in the uptake of atmospheric  $\text{CO}_2$ .

## 1 Introduction

The Arctic Ocean plays an important role in the global carbon cycle as a sink for atmospheric carbon dioxide ( $\text{CO}_2$ ) (Bates and Mathis, 2009). ~~The solubility of  $\text{CO}_2$  increases at low temperatures meaning that  $\text{G}_{\text{gas}}$  exchange and  $\text{CO}_2$  carbon~~ drawdown is enhanced in cold polar surface waters ~~because the solubility of  $\text{CO}_2$  increases at low temperatures~~; this is ~~commonly~~ known as the ocean solubility pump (Parmentier et al., 2013). Despite its role as a sink for  $\text{CO}_2$ , the magnitude of  $\text{CO}_2$  uptake by the Arctic Ocean is poorly constrained as the region remains spatially and temporally under-sampled due to difficult seasonal access heavily skewing measurements to the ice-free summer period (DeGrandpre et al., 2020). Additionally, logistical constraints in poorly charted nearshore waters also tend to bias underway  $\text{CO}_2$  measurements to established shipping routes and the deep ocean basins, leaving much of the Arctic coastal zone under-sampled in the ~~Surface~~ [Ocean](#)  $\text{CO}_2$  Atlas (SOCAT v2022) (Bakker et al., 2016). This is not a trivial oversight, given that the Arctic Ocean is encircled by coasts and their associated shelf seas  $\sim 53\%$  of the  $\sim 10.7 \times 10^6 \text{ km}^2$  Arctic Ocean surface area is  $< 200 \text{ m}$  ~~depth~~ [depth](#) (Jakobsson, 2002) (Bates and Mathis, 2009).

The Arctic is already being heavily impacted by climate change (Landrum and Holland, 2020), with potentially devastating impacts on the Inuit and other ~~indigenous~~ [Indigenous](#) communities who live there (Ford et al., 2008). It is not certain how the Arctic carbon system will respond to ~~climate the present~~ changes and how the effects of processes like ocean acidification will manifest and impact Inuit communities. Projecting long-term change in regions with complex biogeochemistry (i.e., the coastal domain) is particularly difficult. To better predict how the Arctic carbon system will change in the future requires baseline measurements, including detailed surveys and regular monitoring of oceanic  $p\text{CO}_2$  that reflect the diverse nature of Arctic marine environments.

The Canadian Arctic Archipelago (CAA) is made up of numerous islands that cover 13% of the Arctic Ocean (Macdonald et al., 2010). ~~The numerous islands account for the Canadian Arctic and account for the bulk of Canada's~~ [having](#) 162,000  $\text{km}$  of [Arctic](#) coastline (Wynja et al., 2015). The islands of the CAA form a complex bathymetry which is important in

determining the circulation in the CAA (Wang et al., 2012). The majority of existing  $p\text{CO}_2$  measurements made in the CAA were collected along the southern route through the Northwest Passage on the research icebreaker *CGGS Amundsen* (Ahmed et al., 2019). This large  $p\text{CO}_2$  dataset was used to estimate a  $-7.7 \pm 4 \text{ Tg C yr}^{-1}$  sink for the CAA during the open water season (Ahmed and Else, 2019). The *CGGS Amundsen*  $p\text{CO}_2$  dataset provides excellent broad spatial coverage of the CAA, but the vast area surveyed was limited in temporal coverage and fine spatial detail. The *CGGS Amundsen* typically only transited through the central straits, channels, gulfs, and seas ~~that make up of~~ the southern ~~route through the~~ Northwest Passage once each summer. The numerous bays and inlets that are off the main channel were not sampled, meaning that local-scale  $p\text{CO}_2$  variability was potentially unaccounted for during the synoptic scale sampling. This small-scale  $p\text{CO}_2$  variability is difficult to predict empirically and may be better observed via regional studies. For example, the model of Ahmed et al. (2019) ~~is was shown~~ to underestimate  $p\text{CO}_2$  by an average of  $\sim 26 \mu\text{atm}$  in Coronation Gulf and Dease Strait regions of the Kitikmeot Sea. Ahmed et al. (2019) ~~postulated that large river inflow in the region may account for divergences from their model. uAhmed et al. (2019), likely due to river inflow. Understanding what caused this deviation from the model whether this is the case~~ warrants further investigation and makes the Kitikmeot Sea a prime location for focused study.

Our understanding of the inorganic carbon system in the Kitikmeot Sea region ~~primarily~~ comes from three distinct sources of measurements. Firstly, the 2010–2016 summertime ship measurements of  $p\text{CO}_2$  in the central channel of the Kitikmeot presented by Ahmed et al. (2019). Their measurements show the region to be slightly undersaturated at the beginning of August, becoming slightly ~~oversaturated-supersaturated~~ in the middle of August through to the middle of September, and then becoming undersaturated again in early October. Coronation Gulf is one of the few areas of the CAA that was consistently observed to be supersaturated with  $\text{CO}_2$  in summer. ~~Oversaturation-Supersaturation~~ of  $p\text{CO}_2$  in Coronation Gulf is likely a result of high summer surface seawater temperatures ( $\text{CO}_2$  thermodynamics mean that a  $1^\circ\text{C}$  temperature ~~increase~~, increases  $p\text{CO}_2$  by 4.23% ~~(Takahashi et al., 1993)~~(Takahashi et al., 1993)) and high river discharge, particularly to the ~~south~~west (Geilfus et al., 2018). The second source of carbonate system measurements in the region are  $\text{CO}_2$  flux observations at the Qikirtaajuk Island observatory ~~in~~ the Finlayson Islands in Dease Strait (Butterworth and Else, 2018). Their measurements from the 2017 ice breakup season through to the summer indicate that there is  $\text{CO}_2$  drawdown, and thus, undersaturation at breakup and for the first two weeks of open water. Near the end of July, the region transitions into a  $\text{CO}_2$  source through to the end of August (Butterworth and Else, 2018). The region reverts to a sink in late August as the sea cools and surface  $p\text{CO}_2$  declines; the region remains a sink until almost full ice cover in November (Butterworth et al., 2022). A similar pattern was observed in the summer of 2018, except notably, when  $p\text{CO}_2$  began to fall in late August the region did not revert all the way back into a sink (Butterworth et al., 2022). The third source of carbonate system measurements are provided by Duke et al. (2021) who report autonomous  $p\text{CO}_2$  measurements at a depth of 7 m from an instrument installed on the Ocean Networks Canada (ONC) underwater sensor mooring in Cambridge Bay between August 2015 and August 2018. The sensor measurements from Cambridge Bay indicate that  $p\text{CO}_2$  is ~~oversaturated-supersaturated~~ in winter and

undersaturated by the start of June at the onset of sea ice melt (Duke et al., 2021). Their measurements show that there is a short period of ~~oversaturation-supersaturation~~ in the middle of August coinciding with increased sea [water](#) temperature, the ocean then quickly returns to a [CO<sub>2</sub>](#) sink and remains undersaturated up until freeze-up (Duke et al., 2021). Duke et al. (2021) ~~confirmed that the biogeochemical measurements at the ONC site were representative of the offshore during most seasons by comparing discrete dissolved inorganic carbon (DIC) and total alkalinity (TA) samples collected at both 2 and 7 m at the ONC platform and an offshore station (B1). The surface stratification at ONC breaks down after the 2 week sea ice melt and river runoff period in early July. After the sea ice melt and river runoff period, DIC, TA, salinity, and temperature values recoreded by the ONC mooring are then once again representative of the surface mixed layer.~~

All three sources of measurements indicate that there is notable interannual variability in surface  $p\text{CO}_2$  in the Kitikmeot Sea. The ship-based measurements provide a snapshot of spatial variability across the wider region during the open-water season whereas the time series from Qikirtaarjuk Island observatory and the ONC mooring provide insights into seasonal and interannual variability at specific locations. There are obvious shortcomings to both approaches. Icebreaker-based studies may under-represent small-scale variability that exists in nearshore regions that are inaccessible due to the vessel's large draft. Whereas the fixed observatories may over-represent temporal variability which is location-specific; for example, the ONC mooring is in an enclosed Bay close to the outlet of a [large](#)-river (Manning et al., 2020) and the flux footprint of the Qikirtaarjuk Island observatory spans a hotspot for mixing and productivity (Dalman et al., 2019). Given the limitations of each of these data sources, there is a need to understand how representative ~~these data sources~~ [they](#) are of the wider Kitikmeot Sea region.

In this paper, we present surface  $p\text{CO}_2$  measurements made during annual summertime surveys of the Kitikmeot Sea between 2016 and 2019. We use these new  $p\text{CO}_2$  measurements to determine the magnitude of  $\text{CO}_2$  uptake in the Kitikmeot Sea shortly after ice breakup. These new  $p\text{CO}_2$  measurements ~~also~~ allow us to bridge the gap between previous measurements, which were made at contrasting spatial scales (e.g., the low spatial variability point-scale observation from the local carbon observatories and the large-scale CAA-wide  $p\text{CO}_2$  measurements). We use our new measurements to explore whether there are small-scale regional  $p\text{CO}_2$  differences in the inlets and bays of the CAA which are not adequately represented by CAA-wide sampling. We also use our new measurements to explore  $p\text{CO}_2$  variability in the proximity of these observatories to ~~see~~ [determine](#) whether they are representative of the wider region. In attempting to unify existing measurements, we aim to unravel the seasonal and interannual variability of  $p\text{CO}_2$  in the region.

## 130 2 Methods

### 2.1 Oceanographic setting

The Kitikmeot Sea (Figure 1) is a shallow shelf sea within the CAA that encompasses Coronation Gulf to the west, linked via Dease Strait to Queen Maud Gulf in the East, Bathurst Inlet to the South, and Chantrey Inlet to the Southeast (Williams et al., 2018). The communities of Cambridge Bay, Kugluktuk, and Gjoa Haven, Nunavut, are the main year-round settlements in the Kitikmeot Sea region. River inputs from mainland Canada and snow and ice melt provide a considerable source of freshwater in the region (Williams et al., 2018), resulting in some of the lowest salinity surface waters in the CAA (Ahmed et al., 2019). The Kitikmeot sea is nutrient-limited (Back et al., 2021), and as a result chlorophyll concentrations are also low in the region (Kim et al., 2020). Modelling ~~results of the physical oceanography of the region suggest demonstrates~~ that the stratification regime in Dease Strait and Queen Maud Gulf is characterised by a ~40 m warm fresh surface layer and a cold salty bottom layer which extends down to around 100 m (Xu et al., 2021). Coronation Gulf has a three layer regime composed of a 40 m warm fresh surface layer, a colder salty layer down to 100 m and a stable deep layer down to 350 m (Xu et al., 2021). Vertical mixing in the Kitikmeot Sea is prohibited by strong stratification throughout most of the year; however after sea ice breakup wind driven mixing gradually deepens the surface mixed layer resulting in an almost fully mixed water column in Dease Strait (Xu et al., 2021).

The oceanographic boundary for the Kitikmeot Sea has been designated as where the shelf shoals to <30 m in the west (Dolphin and Union Strait) and northeast (Victoria Strait) (Williams et al., 2018). At the Dolphin and Union Strait, warm fresher surface seawater flows out across the sills ~~while and~~ subsurface flows of more saline nutrient-rich Pacific waters enter the sea. Another feature of the Kitikmeot Sea is that strong tidal currents in narrow channels can keep certain areas ice-free in winter (Williams et al., 2018). Strong tidal currents beneath sea ice such as around the Finlayson Islands in Dease Strait act to slow winter sea ice growth and enhance primary production by introducing nutrients (Dalman et al., 2019). First-year sea ice dominates the Kitikmeot Sea although some multiyear ice may be blown into Queen Maud Gulf from the northern part of the CAA (Xu et al., 2021). Seawater temperatures across the Kitikmeot Sea vary considerably throughout the year; they are around -2°C in winter and reach upwards of 10°C in summer (Xu et al., 2021). The bounding sills, large freshwater inputs and low nutrient loads make the Kitikmeot Sea unique within the CAA.

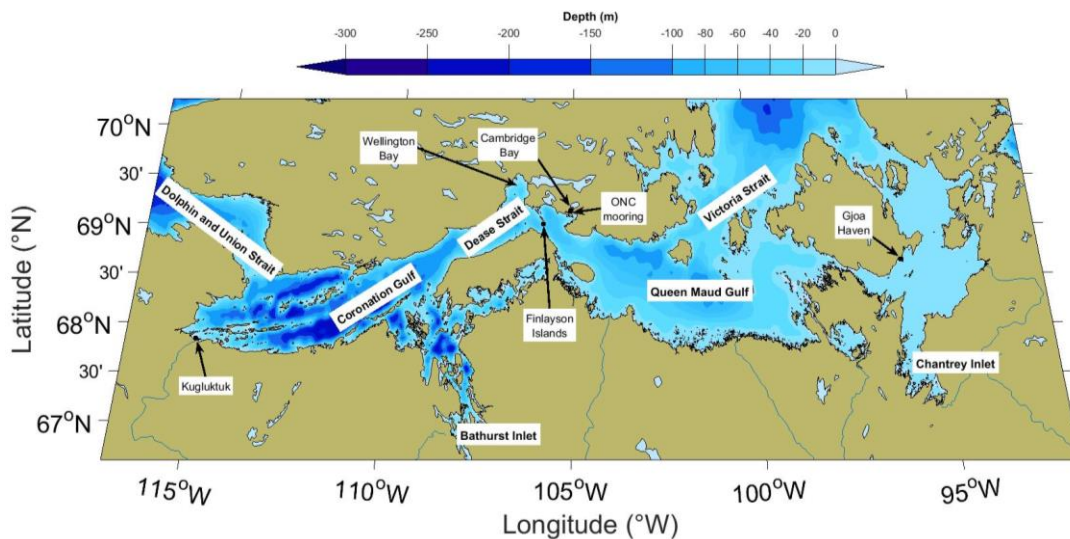


Figure 1: A map of the Kitikmeot Sea. The main settlements in the region (Cambridge Bay, Kugluktuk and Gjoa Haven) are labelled as are the Ocean Networks Canada mooring and the Qikirtaajuk Island observatory where the eddy covariance tower is located. Shoreline data ~~is was taken~~ from the World Vector Shoreline database and river data ~~is was~~ taken from the CIA World Data Bank II (WDBII), both of which were accessed via the Global Self-consistent, Hierarchical, High-resolution Geography Database (GSHHG) (Wessel and Smith, 1996). Bathymetry data ~~is was~~ taken from the 2-minute Gridded Global Relief Data (ETOPO2) v2 database (NGDC, 2006). This map was made using tools from the M\_Map Matlab plotting package (Pawlowicz, 2020).

## 2.2 Field campaign description

Annual oceanographic surveys of the summertime surface seawater partial pressure of carbon dioxide ( $p\text{CO}_2$  (sw)) were conducted between 2016 and 2019 in the Kitikmeot Sea (Figure 1) aboard the *RV Martin Bergmann* as part of the Marine Environmental Observation, Prediction and Response Network (MEOPAR) and Kitikmeot Sea Science Study (K3S) programs (cruise details in table S1). In each of the four years, an underway  $p\text{CO}_2$  system was deployed on cruises conducted under ice-free conditions between early August and mid-September. The Canadian High Arctic Research Station (CHARS) in Cambridge Bay, Nunavut acted as a staging ground for this work ~~since as~~ Cambridge Bay is the home port for the *RV Martin Bergmann*.

Between 2016 and 2019, the cruise track varied from year to year depending on the ~~focus of the work~~ objectives of the research conducted (Figure 2). The first week of each summer field season was typically used to complete work for the MEOPAR program, the majority of the ship time ~~for the MEOPAR work~~ was spent in the proximity of Cambridge Bay, the Finlayson Islands, Wellington Bay and the western region of Queen Maud Gulf. Cruises in mid to late August were used to

170 | conduct work for the K3S program; ~~for the K3S work~~ the ship typically ~~ventured-travelled~~ further ~~from Cambridge Bay~~ field heading into Bathurst Inlet, the central region of Queen Maud Gulf and ~~Chantry~~Chantrey Inlet. The opportunistic nature of the data collection meant that data density varied between regions, as not every region was surveyed each year.

175 | Sea ice concentrations in the months preceding each annual survey ~~are~~were taken from the daily gridded 3.125 km AMSR2 satellite radiometer product (Spreen et al., 2008). To determine weeks since open water, the nearest point on the AMSR2 grid was determined for each  $p\text{CO}_2$  (sw) measurement. The time between the measurement and when sea ice concentration fell constantly below the threshold value for the marginal ice zone (85%) (Cruz-García et al., 2021) was then calculated.

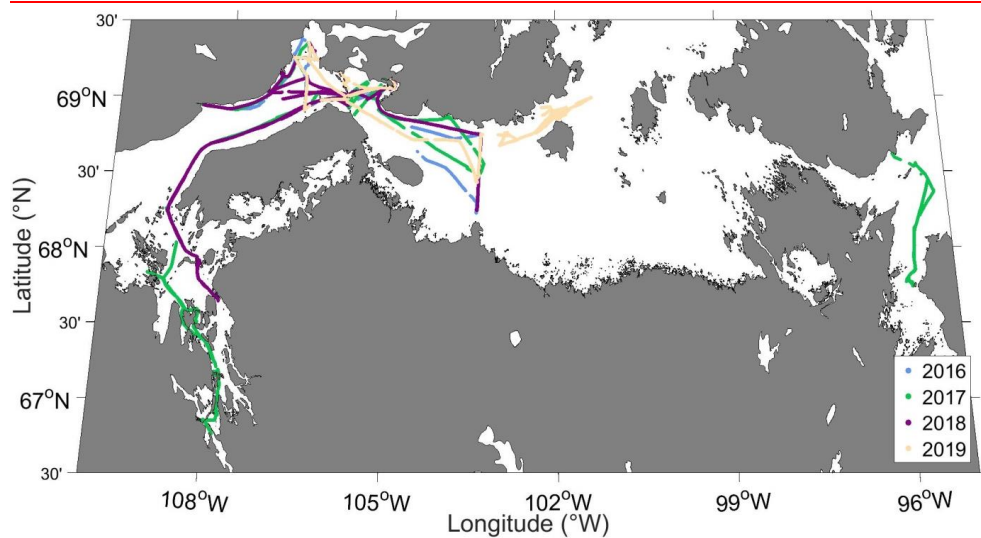
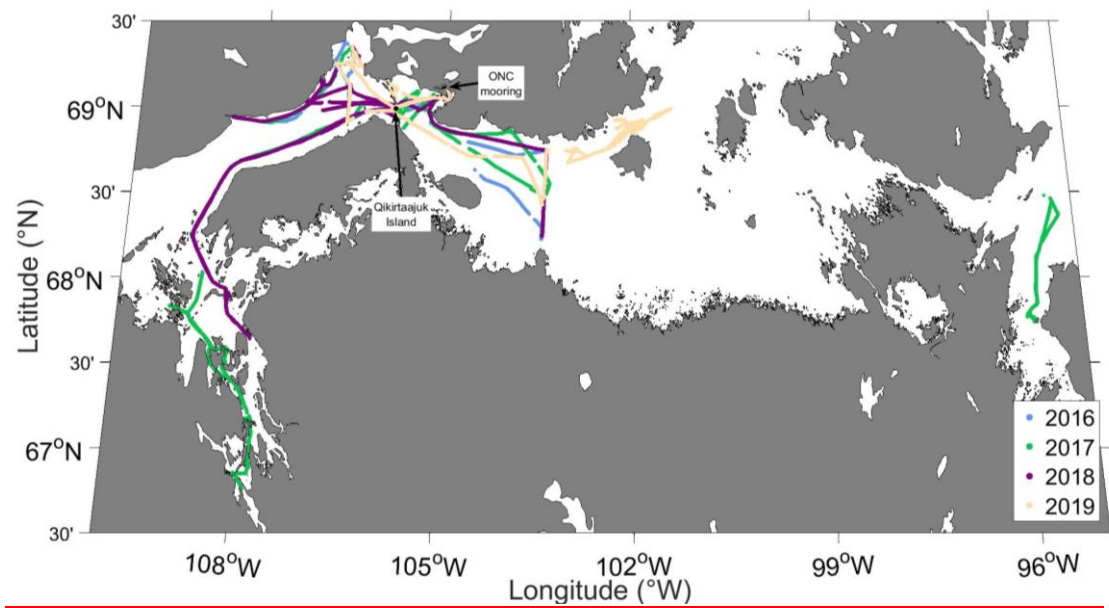


**Figure 2: Ship cruise tracks for each of the four surveyed years. The Ocean Networks Canada mooring and the Qikirtaajuk Island observatory where the eddy covariance tower is located are shown by black dots.**



### 2.3 Underway system

The *RV Martin Bergmann* is a 20 m repurposed commercial fishing trawler from Newfoundland with a draft of 3.4 m (Figure 3a and 3b). The ship does not have its own dedicated integrated underway system; instead surface seawater was sampled from an inlet at a depth of ~1 m through ~2 m of 1/2" ID PVC tubing securely draped over the bulwark of the vessel through an external hatch (Figure 3c and 3d). A Waterra Tempest WSP-12V-3 submersible pump was used to pump surface seawater through this inlet tubing at a rate of 10 L min<sup>-1</sup>. *In situ* surface seawater temperature (SST<sub>(1m)</sub>) was measured by a Campbell Scientific 107 temperature sensor attached to the tubing inlet.

Upon entering the ship, the flow of seawater passed through a SoMAS MSRC VDB-1 vortex debubbler and was ~~then~~ split between several instruments via Tygon tubing (Figure 3). ~~The~~ ~~An~~ Idronaut Ocean Seven 315 On-line module thermosalinograph measured seawater temperature (SST<sub>(tsg)</sub>) and salinity at a seawater flowrate of 0.5 L min<sup>-1</sup>. ~~The~~ ~~A~~ Wetlabs ECO BBFL2B Triplet measured fluorescence at a flowrate of 2.5 L min<sup>-1</sup>. ~~The~~ ~~The output of the~~ ECO fluorescence sensor ~~output~~ was post-processed to remove spikes from bubbles and particles but was not calibrated against *in situ* measurements. A flow of 2 L min<sup>-1</sup> was directed to the seawater equilibrator. Instrument flowrates were set with manual flowmeters so that the internal instrument volumes and associated tubing of the Idronaut, ECO and equilibrator were flushed at the same rate, this meant that approximately half of the 10 L min<sup>-1</sup> flow from the pump was not analysed and was discarded overboard.

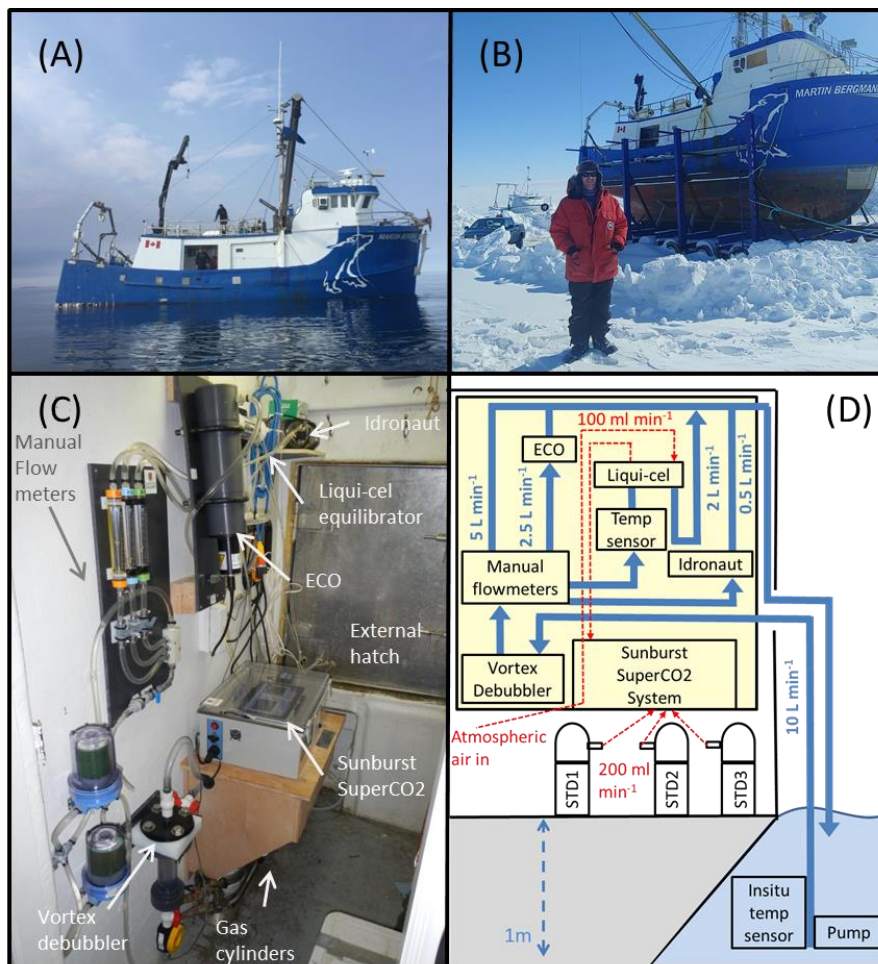


Figure 3: (a) Image of the RV *Martin Bergmann* at sea taken in August 2017, (b) image of RV *Martin Bergmann* stored on its trailer taken on a mild day in May 2019, (c) labelled photograph of the underway system installed in the ship's lab space, and (d) detailed cross sectional schematic of the underway system with labelled instruments and flowrates. Instruments mounted to the wall are shown with a yellow background, water circulation is shown in blue and air circulation is shown in red.

A [made-to-order commercially available](#) Sunburst Sensors underway SuperCO<sub>2</sub> system measured surface seawater CO<sub>2</sub>; [this an identical](#) system was previously described by Evans et al. (2019), ~~and~~. [The SuperCO<sub>2</sub> system](#) follows the general recommendations of Dickson et al. (2007) SOP5. A Permapure liqui-cel 2.5X8 series membrane contactor ~~served was used~~

200 as the equilibrator for the  $p\text{CO}_2$  system, the waterside seawater flowrate for the equilibrator was approximately  $2 \text{ L min}^{-1}$ . Seawater temperature was measured at the equilibrator seawater inlet using a thermistor ( $T_{(\text{equ})}$ ). The gas counter flow into the equilibrator was supplied by an air pump at a flowrate of  $100 \text{ ml min}^{-1}$ .  $\text{CO}_2$  has been shown to fully equilibrate in this model liqui-cel when set up in a single pass setup at these water and gas flowrates (Sims et al., 2017). The system does not utilise a dryer and thus ~~does not require~~ a water vapour correction in post-processing as the equilibrator is assumed to be at  
205 100 % humidity. For additional accuracy, the inbuilt  $\text{H}_2\text{O}$  sensor was calibrated with a LI-610 Portable Dew Point Generator on-site before each deployment. The Super $\text{CO}_2$  system has a standard multi-position valve and alternates between equilibrator air, atmospheric samples, and three gas standards. The timing of the valve switching was set so that each of the three  $\text{CO}_2$  standards ( $\text{CO}_2$  mixing ratios ( $\gamma\text{CO}_2$ ) of 255.1, 409.9, and 566.4) were flushed through the system at  $200 \text{ ml min}^{-1}$  for 5 minutes every 6 hours. Standard gases were certified at the University of Manitoba against standards obtained from  
210 Environment and Climate Change Canada, and are thus traceable to World Meteorological Organization standards. The Super $\text{CO}_2$  system has an integrated air pump configured to make atmospheric measurements; these measurements were not used due to contamination from the ship's exhaust. The Super $\text{CO}_2$  system also measure~~s~~ atmospheric pressure  $P_{(\text{atm})}$ .

Formatted: Subscript

~~Variables Measurements from the underway system~~ were logged every minute.  ~~$\gamma\text{CO}_2$~~  and related variables were logged to  
215 the computer of the Super $\text{CO}_2$  system, the data recorded by the ECO were logged to a separate data file, and the latitude and longitude recorded with a Garmin GPS16X-HVS GPS unit were logged to a Campbell Scientific CR300 data logger. The  $\text{CO}_2$  measured by the system ~~was were~~ processed following ~~SOP 5~~ (Dickson et al., 2007) ~~-SOP 5. Partial pressure of  $\text{CO}_2$  ( $p\text{CO}_2$ ) is measured the output provided by by the Licor 850 in the Super $\text{CO}_2$  system, this is converted to the gas mixing ratio of  $\text{CO}_2$  ( $\gamma\text{CO}_2$ ) using the pressure in the Licor ( $P_{(\text{licor})}$ ). The  $\gamma\text{CO}_2$  is calibrated using a piecewise linear interpolation in~~  
220 ~~time with the three standards. As there was no dryer the equilibrator is assumed to be at full humidity, the partial pressure in the equilibrator ( $p\text{CO}_2_{(\text{equ})}$ ) is was therefore then determined in the equilibrator ( $p\text{CO}_2_{(\text{equ})}$ ) using the calculated by multiplying by atmospheric pressure  $P_{(\text{atm})}$  and assuming full humidity.  $p\text{CO}_2_{(\text{equ})}$  is was~~ converted to  $p\text{CO}_2_{(1\text{m})}$  using the  $T_{(\text{equ})}$ ,  $\text{SST}_{(1\text{m})}$ , and the fractional temperature change constant of (Takahashi et al., 1993). The depth of the seawater inlet was validated each year by comparing the thermosalinograph salinity and the in situ temperature sensor with surface temperature  
225 and salinity from CTD rosette measurements at the surface. ~~As there was no in situ temperature sensor during the 2017 and 2018 field seasons, the warming was then characterised from  $T_{(\text{equ})}$  and CTD rosette measurements following Ahmed et al. (2019), details of this can be found in the supplementary materials. Additionally, median observational values of  $-0.17^\circ\text{C}$  and  $+0.1$  were added to the in situ temperature and salinity to account for ubiquitous skin effects when calculating interfacial seawater  $p\text{CO}_2$  (Woolf et al., 2019),~~  
230

Formatted: Subscript

Formatted: Font:

Using an identical setup, DeGrandpre et al. (2020) estimate the  $p\text{CO}_2$  uncertainty as  $\pm 5 \mu\text{atm}$ , this is the uncertainty for our 2016 and 2019 measurements. In 2017 and 2018, there is an additional uncertainty component associated with using an empirical relationship to obtain  $\text{SST}_{(1\text{m})}$ . This additional uncertainty ~~is was~~ calculated by taking the RMSD values from those

empirical relationships (2017 = 0.49°C, 2018 = 0.64°C) and propagating them through the temperature equation for  $p\text{CO}_2(1\text{m})$  (Takahashi et al., 1993). This ~~results~~resulted in an additional 2.09% and 2.74% uncertainty in  $p\text{CO}_2(1\text{m})$ , these values are similar to the 2% uncertainty reported by (Ahmed et al., 2019) following the same method. For a  $p\text{CO}_2(\text{equ})$  value of 300  $\mu\text{atm}$  this equates to an additional 6.3 and 8.2  $\mu\text{atm}$  uncertainty for each year respectively. Propagating uncertainties gives ~~final~~average uncertainties of 8.04 and 9.60  $\mu\text{atm}$  for 2017 and 2018 respectively. ~~These~~ calculation of the 2017 and 2018 ~~se~~ uncertainties is consistent with the International Bureau of Weights and Measures (BIPM) Guide to the expression of uncertainty in measurement (GUM) methodology (JCGM, 2008).

The standard system configuration during the four cruises is detailed above; changes from this configuration during specific cruises are detailed in the supplementary materials (Table S2). There are several logistical aspects associated with deploying, operating, and maintaining an underway  $p\text{CO}_2$  system in a remote Arctic location on a small vessel like the *RV Martin Bergmann*; this is discussed further in supplementary materials.

#### 2.4 Calculations: ~~Air-Air~~sea $\text{CO}_2$ fluxes

In the absence of a reliable ship-based atmospheric  $\text{CO}_2$  record, hourly measurements ~~are~~were taken from the atmospheric observatory in Barrow Alaska (71.32°N, 156.61°W) (K.W. Thoning, 2020; Peterson et al., 1987). Despite the long distance between Barrow and the Kitikmeot Sea (around 1800 km), atmospheric  $\text{CO}_2$  ~~should be~~are quite~~very~~ similar at both locations as the atmosphere is well mixed for a long residence time gas like  $\text{CO}_2$  and both locations are remote northern sites away from biogenic and industrial emissions. To validate this assumption a long term (1985–2019) mean difference of 0.246  $\mu\text{atm}$  was calculated between the hourly measurements at Barrow and weekly atmospheric samples from Alert Nunavut (Lan et al., 2022). Wind speed adjusted to a reference height of 10 m ( $U_{10}$ ) ~~is~~was taken from the Qikirtaajuk Island observatory (Butterworth and Else, 2018) for the 2017 and 2018 field seasons whereas a four times daily record of  $U_{10}$  from the NCEP-DOE v2 reanalysis product (Kalnay et al., 1996) ~~is~~was used for 2016 and 2019 field seasons.

The air~~-~~sea fluxes of  $\text{CO}_2$  ( $F$ ,  $\text{mmol m}^{-2} \text{d}^{-1}$ ) ~~is~~was calculated as

$$F_{(\text{sea-air})} = k_w k_0 \Delta p\text{CO}_2 \text{ SF}$$

The water phase gas transfer velocity ( $k_w$ ,  $\text{cm hr}^{-1}$ ) ~~is~~was calculated using  $U_{10}$  and the parameterisation of Nightingale et al. (2000), a unitless Schmidt number ( $Sc$ ) normalised to a  $Sc$  of 660 (Wanninkhof, 2014) ~~is~~was used to scale  $k_w$ .

$$k_w = (0.222 (U_{10})^2 + 0.333 (U_{10})) (Sc/660)^{-1/2}$$

$\Delta p\text{CO}_2$  ( $\mu\text{atm}$ ) is the partial pressure difference between the seawater interface and air  $\Delta p\text{CO}_2 = p\text{CO}_2(\text{sw}) - p\text{CO}_2(\text{air})$ . The solubility of  $\text{CO}_2$  in seawater ( $k_0$ ,  $\text{mol L}^{-1} \text{atm}^{-1}$ ) ~~is~~was taken from (Weiss, 1974). A unit scaling factor (SF) of 0.24 is used to convert the units of  $k_w$  to  $\text{md}^{-1}$ . The Schmidt number and solubility ~~are~~were calculated using the *in situ* temperature and salinity values adjusted for skin effects (Woolf et al., 2019).

265

270 Direct measurements of the air–sea CO<sub>2</sub> fluxes ( $F_{(sea-air)}$ ) made using the micrometeorological eddy covariance technique (Butterworth and Else, 2018) ~~can be used~~ used to infer  $pCO_{2(sw)}$  by rearranging the flux equation. ~~That was achieved as follows~~ using  $pCO_{2(air)}$  from the Licor 7200 at the Qikirtaarjuk Island observatory and SST and SSS from a mooring at a depth of 13 m which was 1 km from the tower (Butterworth et al., 2022). ~~An eddy covariance flux footprint is the area over which the eddy covariance measurements correspond to and varies depending on atmospheric conditions. Using the Kljun et al. (2015) footprint model, Butterworth and Else (2018) showed that the footprint of the Qikirtaarjuk Island observatory during spring and summer can be modelled as an ellipse with an upwind axis that varies between approximately 0.75 – 2.0 km and a cross-wind axis that varies between 0.1 – 0.2 km. The effective flux footprint is however much smaller as over 90% of the flux signal comes from within 100 m of the tower. Uncertainty in the  $pCO_{2(sw)}$  values derived using eddy covariance arises from uncertainty in the flux measurements (hourly uncertainty of ~20% in the Arctic) (Dong et al., 2021a), uncertainty in the gas transfer parameterisation (~ 5–10%) (Woolf et al., 2019), the small uncertainty in the atmospheric  $pCO_2$  value, uncertainties in  $k_0$  and the schmidt number (including uncertainties in SST and salinity inputs from the 13 m mooring).~~

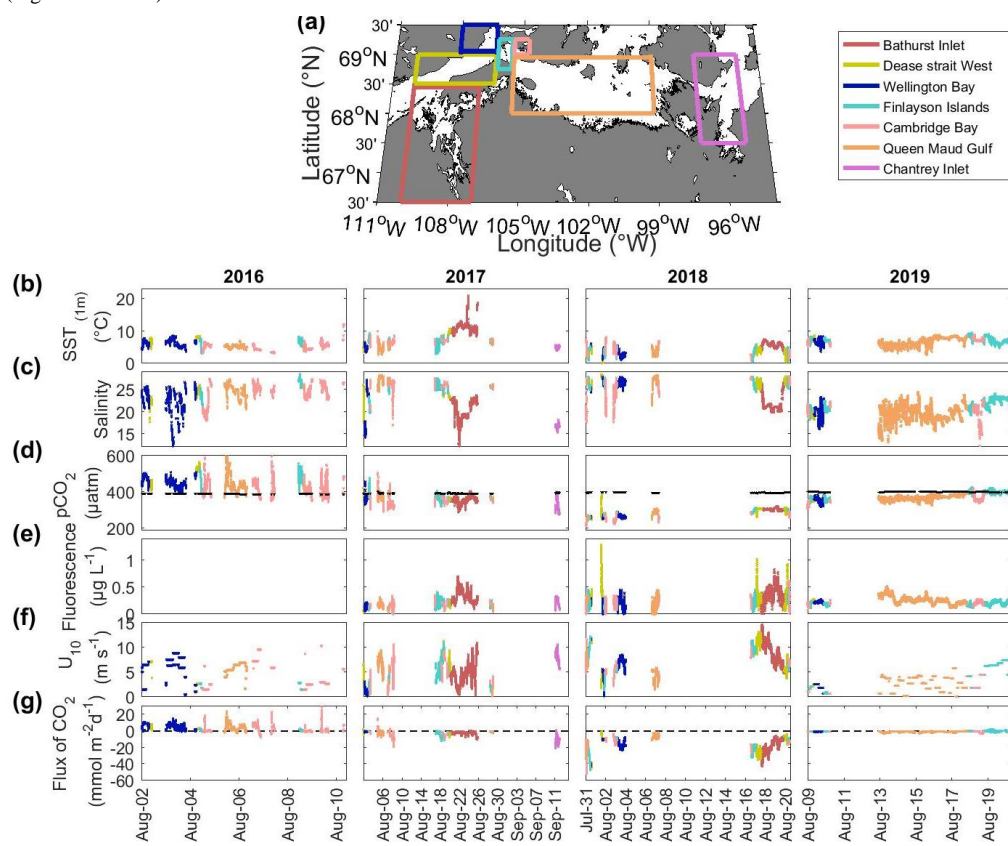
$$280 (F_{(sea-air)} / k_w k_0 \text{ SF}) + pCO_{2(air)} = pCO_{2(sw)}$$

### 3. Results

285 To facilitate comparisons between ~~the four summertime~~ cruises ~~made in different years~~, observations have been partitioned into separate oceanographic zones based on the local geography, observational data density, previous  $pCO_2$  (sw) measurements, and proximity to the local carbon observatories (Figure 4a). Bathurst Inlet and Chantry Inlet were designated zones based on their large freshwater inputs. The Finlayson Islands and Cambridge Bay are where the Qikirtaarjuk Island observatory and ONC mooring are located, respectively; these regions were also heavily surveyed because the *RV Martin Bergmann* often returned to port in Cambridge Bay and passed the islands to access Wellington Bay and Bathurst Inlet. Wellington Bay (Figure 1) is a shallow, partially enclosed basin for which a relatively large amount of data was collected due to annual fish-tagging surveys associated with the local subsistence char fishery (Harris et al., 2020).  
290 All the measurements in the Dease Strait West zone were made in the central channel and are in the same approximate geographical region to those collected by Ahmed et al. (2019). Most of the measurements in the Queen Maud Gulf zone were made in the west; the box is large enough to include sparse measurements in the central and Northern regions which do not warrant being considered separately.

295 Observations of temperature, salinity,  $pCO_{2(sw)}$ , fluorescence,  $U_{10}$ , and CO<sub>2</sub> flux during the four field seasons are plotted as time series and coloured by the sub-region of the measurement (Figure 4b-4g). Summary statistics (mean, standard deviation, and range) of each variable in each region for all four cruises are presented in Table 1. Plots showing the timing of

the cruise track, temperature, salinity,  $p\text{CO}_{2(\text{sw})}$ , and chlorophyll-a fluorescence can be found in the supplementary materials (Figures S2 to S6).



300

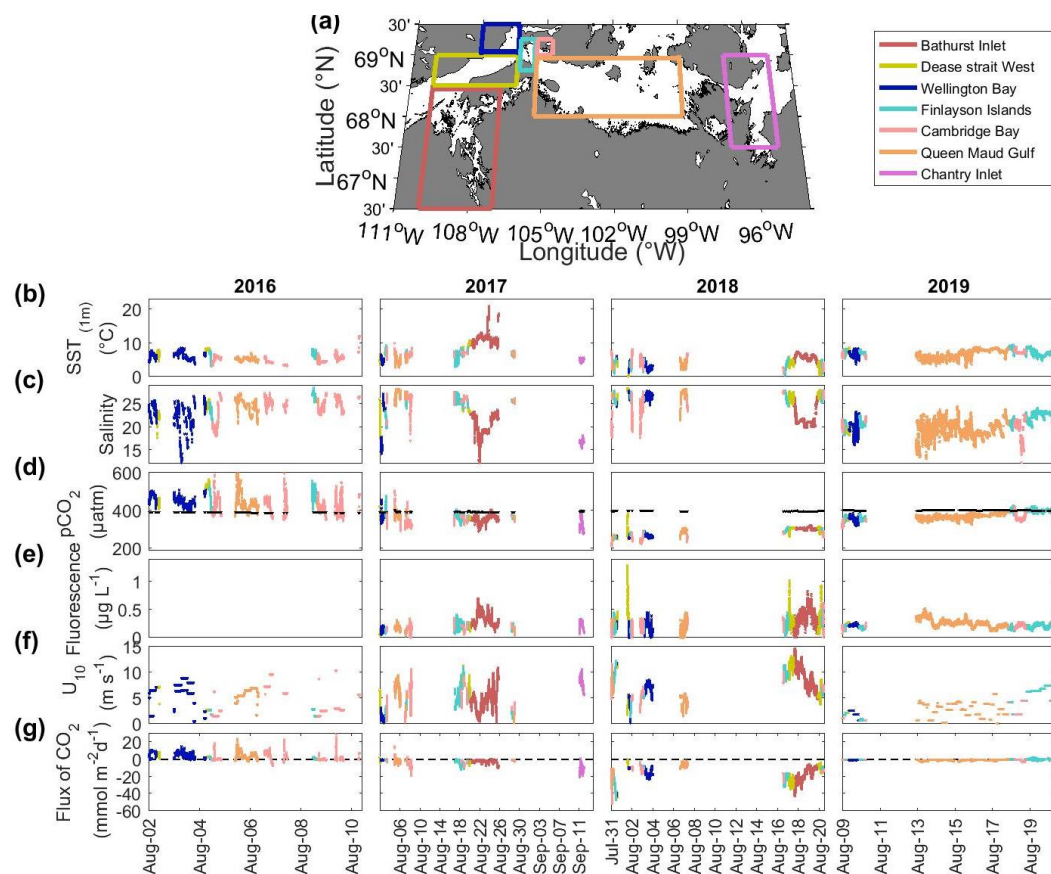


**Figure 4:** (a) Map of Kitikmeot Sea showing the region surveyed by the *RV Martin Bergmann* between 2016 and 2019. The sampled region was subdivided as described in the main text; these sub regions are shown as coloured boxes and correspond to the names in the legend. Timeseries subplots of underway surface ocean (1m) observations for 2016 through to 2019 of (b) SST (1m), (c) salinity, (d)  $p\text{CO}_2$  (sw) (with  $p\text{CO}_2$  (atm) in black), (e) fluorescence, (f)  $U_{10}$ , and (g) flux of  $\text{CO}_2$  (no flux is indicated by a dashed black line). The time series data are coloured according to the sampling regions in panel (a). The period of measurements was not consistent between years so the date label tick spacing and the range are different between years. Large data gaps correspond to when the ship was in port between cruise legs or data outages. [An alternate version of this figure where the y-axes are not normalised between years is included in the supplement \(Figure S7\).](#)

$\text{SST}_{(1\text{m})}$  interannual variability was on the order of several degrees (Figure 4b), for example the  $\text{SST}_{(1\text{m})}$  was lowest in 2018 (4.3 °C) was cooler than  $\text{SST}_{(1\text{m})}$  and highest in 2017 (8.4 °C) (Table 1). Inter-region  $\text{SST}_{(1\text{m})}$  differences of  $\sim 10^\circ\text{C}$  were observed during all four surveys, for example in 2016 the range is  $\text{SST}$  was 3.18 – 12.13°C (Figure 4b Table 1). Summertime warming of several degrees can be observed in the data for certain sub regions which were visited multiple



305 times such as Cambridge Bay in ~~2016–2016~~ (SST<sub>(1m)</sub> trend of +0.11 °C d<sup>-1</sup> from the 5<sup>th</sup> to 10<sup>th</sup> August 2016) ~~and or were~~  
~~sampled for a continuous period such as~~ Queen Maud Gulf in 2019 (SST<sub>(1m)</sub> trend of +0.64 °C d<sup>-1</sup> from the 13<sup>th</sup> to 19<sup>th</sup>  
310 ~~August 2019~~) (Figure 4b). Some of the sub regions were considerably warmer than others (e.g., Bathurst Inlet ~~was 2.82 °C~~  
~~warmer in 2017 and 1.51 °C warmer in 2018 compared to the measurement averages for those respective years in 2017 and~~  
~~2018~~), whereas other regions ~~were consistently colder like Queen Maud Gulf were consistently colder (e.g., Queen Maud~~  
~~Gulf was 3.45 °C colder in 2017 and 0.76 °C colder compared to the measurement averages for those respective years)~~  
~~(Table 1).~~

There was large interannual variability in surface salinity; for example ~~average observed~~ salinity in 2019 was ~~20.12 generally~~  
~~lower than compared with 24.82 in~~ 2018 (Figure 4c). Salinity values were much lower in ~~ChantryChantrey~~ Inlet in 2017  
315 ~~(16.61)~~ and Bathurst Inlet in both 2017 ~~(20.78)~~ and 2018 ~~(21.86)~~ relative to the salinities in other regions in those years  
(Table 1). Salinity ranges on the order of ~10 were observed between regions in all years, ~~for example in 2018 the maximum~~  
~~salinity range was 10.84 °C~~. The salinity data are marked by rapid changes of ~5 which did not coincide with equivalent  
temperature changes (Figure ~~3e4c~~); these salinity transitions are evident in the 2017 and 2018 Bathurst Inlet data, much of  
the Cambridge Bay data and the Wellington Bay data from 2016 and 2019. There is evidence of freshening in ~~Wellington~~  
320 ~~Bay from the 2<sup>nd</sup> to 4<sup>th</sup> August the first week of August 2016 (salinity trend of -0.87 d<sup>-1</sup>) and in Queen Maud Gulf in 2019~~  
~~(salinity trend of 0.11 d<sup>-1</sup> from the 13<sup>th</sup> to 19<sup>th</sup> August 2019)~~, but there does not appear to be a seasonal freshening trend in  
2017 or 2018.

There was high interannual  $p\text{CO}_2$  (sw) variability (Table 1), ~~where average measured~~  $p\text{CO}_2$  (sw) was ~~close to equilibrium with~~  
325 ~~the atmosphere supersaturated (445  $\mu\text{atm}$ ) in 2016, undersaturated in and highly undersaturated in 2017 (361  $\mu\text{atm}$ ), 2018 and~~  
~~2019 (373  $\mu\text{atm}$ ) and highly undersaturated in 2018 (288  $\mu\text{atm}$ ) 2019~~ (Figure 4d). ~~There was also high regional variability in~~  
~~large~~  $p\text{CO}_2$  (sw) ~~interannual variability was larger than the observed regional variability~~ each year, ~~for example in 2018~~  $p\text{CO}_2$   
~~(sw) ranged from 218  $\mu\text{atm}$  to 387  $\mu\text{atm}$  (Table 1). There were identifiable trends in~~  $p\text{CO}_2$  (sw) across all regions in 2018 and  
330 ~~2019 (Figure 4d); for example,  $p\text{CO}_2$  (sw) increased by 2.22  $\mu\text{atm d}^{-1}$  from the 31<sup>st</sup> July to 21<sup>st</sup> August 2018 and 4.04  $\mu\text{atm d}^{-1}$~~   
~~from the 9<sup>th</sup> to 21<sup>st</sup> August 2019, across all regions in both 2018 and 2019; this is also seen as increases on return visits to the~~  
~~Finlayson Islands and Cambridge Bay several weeks apart from each other (Figure 4d).~~ In all four years, Cambridge Bay had  
lower  $p\text{CO}_2$  (sw) relative to the other regions, ~~for example the average  $p\text{CO}_2$  (sw) in Cambridge Bay in 2019 was 359  $\mu\text{atm}$~~   
~~whereas the averages in the Finlayson Islands and Queen Maud Gulf were 392  $\mu\text{atm}$  and 370  $\mu\text{atm}$  respectively (Table 1).~~  
Low  $p\text{CO}_2$  (sw) values were also seen in Bathurst Inlet (e.g., 359  $\mu\text{atm}$  in 2017), ~~ChantryChantrey~~ Inlet (e.g., 326  $\mu\text{atm}$  in  
335 ~~2017)~~ and Wellington Bay (e.g., 268  $\mu\text{atm}$  in 2018) (Table 1). Many low  $p\text{CO}_2$  (sw) regions were also low salinity regions, ~~for~~  
~~example ChantryChantrey Inlet and Wellington Bay in 2017 (Table 1).~~ Fluorescence was generally low throughout all the  
cruises, in all years, except for the relatively higher fluorescence signal in Bathurst Inlet and around the Finlayson Islands  
(Figure 4e). The air–sea  $\text{CO}_2$  flux (Figure 4g) reflects the trends in the predictor variables, particularly  $p\text{CO}_2$  (sw) and  $U_{10}$

Formatted: Subscript



(Figure 4d and 4f). The air–sea flux calculated in 2016 was ~~small~~ ~~(3.58 0.41)~~  $\text{mmol m}^{-2} \text{d}^{-1}$  reflecting the fact that the  $p\text{CO}_2$  (sw) was ~~close to equilibrium supersaturated with the atmosphere.~~ In 2017 and 2019, surface ocean  $p\text{CO}_2$  (sw) was quite undersaturated (~~309–361~~ and ~~3330–73~~  $\mu\text{atm}$  respectively), the 2017 flux was larger (~~-2.96 -7.7~~  $\text{mmol m}^{-2} \text{d}^{-1}$ ) than the 2019 flux (~~-0.57 -2.1~~  $\text{mmol m}^{-2} \text{d}^{-1}$ ) as the wind speed was very low in 2019 ( $3.1 \text{ ms}^{-1}$ ). As  $p\text{CO}_2$  (sw) was highly undersaturated (288  $\mu\text{atm}$ ) in 2018, there was a large flux into the ocean -16.79  $\text{mmol m}^{-2} \text{d}^{-1}$ .

Table 1: Underway surface ocean (1m) observation summary table for the *RV Martin Bergmann* cruises from 2016 through 2019. Geographical sub regions are defined in Figure 4a. Top line is the mean  $\pm 1$  standard deviation and the bottom row is the measurement range. Table averages are the average of all the observations for each variable for each year and have not been scaled to the spatial extent of each region. ~~Whilst yearly averages are provided, as the spatial extent of the measurements from each year was different, comparisons between years should be made with caution.~~

Year	Sub region	No of obs	SST <sub>(1m)</sub> (°C)	Salinity	$p\text{CO}_2$ (sw) ( $\mu\text{atm}$ )	Fluorescence	$U_{10}$ ( $\text{m s}^{-1}$ )	Flux ( $\text{mmol m}^{-2} \text{d}^{-1}$ )
2016	Dease Strait West	376	7.62 $\pm$	23.58 $\pm$	<del>490.66 <math>\pm</math> 46.38</del>	-	4.25 $\pm$ 2.31	<del>4.37 <math>\pm</math> 1.71</del>
			0.75	1.54	<del>411.51 -</del>		1.12 - 7.22	<del>0.64 -</del>
			4.71 -	17.74 -	<del>567.38444.95</del>			<del>8.770.77 <math>\pm</math></del>
			8.50	26.08	<del><math>\pm</math> 46.08</del>			<del>1.48</del>
					<del>370.10 -</del>			<del>-2.93 -</del>
					<del>519.84</del>			<del>3.10</del>
	Wellington Bay	1523	6.35 $\pm$	22.37 $\pm$	<del>455.98 <math>\pm</math> 26.26</del>	-	6.05 $\pm$ 2.23	<del>5.32 <math>\pm</math> 3.50</del>
			1.10	3.11	<del>393.24 -</del>		0.58 -	<del>-0.23 -</del>
			3.68 -	12.21 -	<del>510.08411.52</del>		8.91	<del>15.190.81 <math>\pm</math></del>
			8.66	26.84	<del><math>\pm</math> 26.57</del>			<del>2.64</del>
					<del>347.26 -</del>			<del>-7.27 -</del>
					<del>463.81</del>			<del>6.38</del>
	Finlayson Islands	412	6.30 $\pm$	25.67 $\pm$	<del>471.05 <math>\pm</math> 40.86</del>	-	2.19 $\pm$ 0.59	<del>1.23 <math>\pm</math> 0.99</del>
			1.46	1.77	<del>383.13 -</del>		1.55 -	<del>-0.15 -</del>
			3.32 -	21.01 -	<del>560.18428.09</del>		2.92	<del>3.380.58 <math>\pm</math></del>
			8.25	28.57	<del><math>\pm</math> 39.42</del>			<del>0.76</del>
					<del>342.34 -</del>			<del>-0.67 - 2.30</del>
					<del>512.69</del>			
	Cambridge Bay	2051	5.18 $\pm$	24.42 $\pm$	<del>423.87 <math>\pm</math> 43.44</del>	-	4.22 $\pm$ 2.69	<del>2.24 <math>\pm</math> 4.45</del>
			1.38	2.29	<del>347.40 -</del>		1.50 -	<del>-7.23 -</del>
3.18 -			18.06 -	<del>656.73384.59</del>		10.37	<del>32.88-0.18 <math>\pm</math></del>	
12.13			27.51	<del><math>\pm</math> 40.72</del>			<del>3.85</del>	
				<del>311.52 -</del>			<del>-13.93 -</del>	
				<del>598.99</del>			<del>23.58</del>	
Queen Maud	1173	5.38 $\pm$	24.61 $\pm$	<del>444.26 <math>\pm</math> 57.26</del>	-	5.93 $\pm$ 1.08	<del>4.24 <math>\pm</math> 4.00</del>	

Formatted: Superscript

Formatted: Superscript

	Gulf		0.56 4.22 – 7.14	1.54 20.71 – 27.37	<del>372.35 –</del> <del>749.17404.92</del> <del>±53.00</del> <del>337.11–</del> <del>687.37</del>		1.55 – 6.97	<del>-2.02 –</del> <del>24.300.75±</del> <del>3.76</del> <del>-5.33–</del> <del>20.06</del>
	Average all	5535	5.80 ± 1.34 3.18 – 12.13	23.93 ± 2.57 12.21 – 28.57	<del>445.08 ± 47.37</del> <del>347.40 –</del> <del>749.17403.65</del> <del>±44.44</del> <del>311.52–</del> <del>687.37</del>	-	4.94 ± 2.45 0.58 – 10.37	<del>3.58 ± 4.08</del> <del>-7.23 –</del> <del>32.880.41±</del> <del>3.32</del> <del>-13.93–</del> <del>23.58</del>
2017	Bathurst Inlet	<del>74267452</del>	<del>11.24 ±</del> <del>1.90</del> <del>11.27±</del> <del>1.96</del> 8.56 – 21.14	20.78 ± 2.04 11.04 – 23.88	<del>358.80 ± 16.47</del> <del>291.75 –</del> <del>407.48302.27</del> <del>±18.57</del> <del>242.22–</del> <del>350.96</del>	0.32 ± 0.12 0.10 – 0.71	<del>4.54 ± 2.22</del> <del>4.56±2.23</del> 0.38 – 10.91	<del>-2.11 ± 1.87</del> <del>-10.32 –</del> <del>0.70-5.80±</del> <del>4.97</del> <del>-26.27–</del> <del>0.12</del>
	Dease Strait West	1137	8.27 ± 1.93 3.40 – 10.60	23.21 ± 1.59 14.63 – 26.04	<del>367.92 ± 6.24</del> <del>352.31 –</del> <del>420.93321.91</del> <del>±10.71</del> <del>301.44–</del> <del>381.48</del>	0.18 ± 0.07 0.04 – 0.29	6.89 ± 2.32 0.30 – 11.43	<del>-3.83 ± 2.24</del> <del>-9.31 –</del> <del>2.55-9.62±</del> <del>5.32</del> <del>-22.07–</del> <del>0.06</del>
	Wellington Bay	847	5.04 ± 0.76 3.55 – 7.20	20.08 ± 4.60 14.23 – 27.22	<del>361.68 ± 15.08</del> <del>334.16 –</del> <del>459.24327.07</del> <del>±13.25</del> <del>300.42–</del> <del>411.75</del>	0.14 ± 0.03 0.07 – 0.22	1.27 ± 0.60 0.29 – 3.12	<del>-0.28 ± 0.24</del> <del>-1.38 –</del> <del>0.34-0.55±</del> <del>0.44</del> <del>-2.34–</del> <del>0.09</del>
	Finlayson Islands	3491	6.95 ± 0.83 3.08 – 9.39	25.18 ± 1.38 19.86 – 27.60	<del>372.81 ± 15.10</del> <del>324.66 –</del> <del>478.13331.18</del> <del>±14.07</del> <del>284.14–</del> <del>418.75</del>	0.20 ± 0.06 0.04 – 0.42	4.53 ± 2.31 0.43 – 11.12	<del>-2.10 ± 2.12</del> <del>-11.51 –</del> <del>0.70</del> <del>-5.05 ± 4.21</del> <del>-20.46–</del> <del>0.00</del>
	Cambridge Bay	1951	6.47 ± 0.73 3.63 – 9.99	26.14 ± 1.48 17.09 – 28.14	<del>350.80 ± 27.19</del> <del>294.77 –</del> <del>506.91</del> <del>313.20 ± 24.52</del> <del>266.37–</del> <del>443.82</del>	0.15 ± 0.06 0.00 – 0.36	5.05 ± 2.46 0.43 – 10.69	<del>-4.08 ± 4.61</del> <del>-18.76 –</del> <del>15.80-7.20±</del> <del>6.36</del> <del>-27.52–</del> <del>6.16</del>
	Queen Maud	1519	4.97 ±	27.25 ±	<del>378.39 ± 11.69</del>	0.17 ± 0.03	6.64 ± 2.28	<del>-1.97 ± 1.73</del>

	Gulf		1.23 2.78 - 7.50	1.05 24.58 - 28.31	<del>346.81</del> <del>422.62</del> <del>342.14 + 10.05</del> <del>314.16</del> <del>376.45</del>	0.07 - 0.32	0.29 - 9.46	<del>-7.11</del> <del>1.76-6.16±</del> <del>2.95</del> <del>-12.76</del> <del>-0.07</del>
	Chantry Inlet	1102+247	4.97 ± <del>0.40</del> <del>4.99 ±</del> <del>0.38</del> 4.09 - 5.76	16.61 ± <del>0.57</del> <del>16.71 ±</del> <del>0.61</del> 15.45 - 18.25	325.91 ± 34.66 <del>280.74 -</del> <del>403.54291.56</del> <del>±31.46</del> <del>250.07</del> <del>363.39</del>	0.22-23 ± 0.06 0.07 - 0.34	8.33 ± 1.15 <del>5.69 -</del> <del>10.738.11</del> <del>±1.31</del> <del>5.18</del> <del>10.73</del>	-11.60 ± <del>4.49</del> <del>-20.77 -</del> <del>1.16-16.55±</del> <del>4.11</del> <del>-26.23</del> <del>-7.18</del>
	Average all	17473+9730	8.42 ± <del>2.95</del> <del>8.00 ±</del> <del>3.07</del> 2.78 - 21.14	22.68 ± <del>3.51</del> <del>22.59 ±</del> <del>3.44</del> 11.04 - 28.31	361.07 ± 22.20 <del>280.74 -</del> <del>506.91308.55</del> <del>±28.80</del> <del>224.83</del> <del>443.82</del>	0.24 ± 0.12 <del>0.23 ± 0.11</del> 0.00 - 0.71	5.02 ± 2.59 <del>5.19 ± 2.61</del> 0.29 - 11.43	-2.96 ± 3.55 <del>-20.77 -</del> <del>15.80-7.70±</del> <del>6.70</del> <del>-29.73</del> <del>6.16</del>
2018	Bathurst Inlet	3215	5.80 ± <del>0.91</del> <del>2.84 -</del> <del>7.515.85</del> <del>±0.92</del> <del>2.86</del> <del>7.58</del>	21.86 ± 1.91 19.81 - 27.52	305.39 ± 5.79 <del>293.75 -</del> <del>322.70274.34</del> <del>±6.07</del> <del>263.43</del> <del>291.23</del>	0.37 ± 0.15 -0.01 - 0.84	8.89 ± 2.27 4.79 - 14.69	-17.58 ± <del>8.01</del> <del>-42.85 -</del> <del>-5.30-23.65</del> <del>±10.81</del> <del>-56.85</del> <del>-6.96</del>
	Dease Strait West	1516	3.28 ± <del>1.80</del> <del>-1.29 -</del> <del>6.033.30</del> <del>±1.82</del> <del>-1.33</del> <del>6.08</del>	26.83 ± 1.01 24.42 - 28.50	298.91 ± 18.93 <del>250.68 -</del> <del>386.92272.02</del> <del>±17.12</del> <del>228.31</del> <del>359.15</del>	0.39 ± 0.25 0.06 - 1.30	8.38 ± 3.07 1.88 - 13.16	-17.89 ± <del>10.91</del> <del>-44.92 -</del> <del>-0.60-22.94</del> <del>±13.81</del> <del>-52.05</del> <del>-1.61</del>
	Wellington Bay	1414	3.03 ± <del>1.21</del> <del>1.23 -</del> <del>6.133.04</del> <del>±1.23</del> <del>1.22</del> <del>6.19</del>	26.73 ± 0.80 24.48 - 27.93	268.16 ± 8.60 <del>253.76 -</del> <del>294.05244.40</del> <del>±7.04</del> <del>232.31</del> <del>266.22</del>	0.20 ± 0.11 -0.16 - 0.46	6.85 ± 2.12 0.28 - 11.90	-17.72 ± <del>7.68</del> <del>-42.44 -</del> <del>-7.81-20.84</del> <del>±9.17</del> <del>-50.83</del> <del>-9.08</del>
	Finlayson Islands	1352	3.23 ± <del>1.47</del> <del>0.47 -</del>	26.62 ± 1.02 24.68 -	284.96 ± 16.21 <del>248.81 -</del> <del>317.35259.49</del>	0.24 ± 0.11 -0.07 - 0.62	8.29 ± 2.36 1.41 - 12.32	-21.20 ± <del>8.83</del> <del>-46.82 -</del>

			5.823.24 ±1.49 0.45— 5.87	28.07	±14.51 228.82— 284.74			-7.29-25.93 ±10.26 -55.55— -9.07
	Cambridge Bay	972	5.02 ± 1.88 1.34 — 8.145.07 ±1.90 1.33— 8.22	23.80 ± 3.11 17.66 — 27.95	253.52 ± 20.43 217.83 — 301.45228.59 ±20.23 193.07— 271.62	0.21 ± 0.11 -0.27 — 0.62	6.23 ± 1.98 2.33 — 11.76	-15.35 ± 9.89 -51.97 — -2.72-17.94 ±11.36 -59.63— -3.19
	Queen Maud Gulf	1043	3.53 ± 0.89 1.87 — 5.723.55 ±0.90 1.87— 5.77	27.06 ± 1.17 21.56 — 28.20	286.50 ± 15.82 250.61 — 310.12260.24 ±14.14 227.45— 282.02	0.18 ± 0.13 -0.19 — 0.45	4.70 ± 1.66 1.61 — 10.31	-7.58 ± 5.98 -34.36 — -0.99-9.17 ±6.82 -39.80— 1.25
	Average all	9512	4.29 ± 1.79 -1.29 — 8.144.32 ±1.82 -1.33— 8.22	24.82 ± 2.83 17.66 — 28.50	288.55 ± 22.12 217.83 — 386.92261.19 ±19.70 193.07— 359.15	0.29 ± 0.18 -0.27 — 1.30	7.70 ± 2.71 0.28 — 14.69	-16.79 ± 9.34 -51.97 — -0.60-21.26 ±11.80 -59.63— -1.25
2019	Wellington Bay	718	6.78 ± 0.97 3.82-81 — 8.56	19.81 ± 1.79 16.08 — 23.35	353.43 ± 14.76 320.60 — 394.70346.29 ±13.72 289.15— 354.95	0.22 ± 0.02 0.17 — 0.28	1.92 ± 0.70 0.64 — 2.64	-0.62 ± 0.25 -1.03 — -0.01-1.15 ±0.49 -1.87— 0.12
	Finlayson Islands	2870	7.37 ± 0.96 4.74 — 9.65	21.72 ± 1.24 18.13 — 24.21	392.03 ± 18.97 320.90 — 427.40346.16 ±15.22 285.01— 376.12	0.20 ± 0.04 0.11 — 0.31	4.82 ± 2.35 0.64 — 7.47	0.02 ± 0.49 -1.89 — 2.35 -3.07 ± 1.95 -7.11— 0.16
	Cambridge Bay	1097	7.20 ± 0.55 5.21 — 8.81	20.03 ± 2.05 12.23 — 22.61	359.27 ± 17.62 308.66 — 418.43346.70 ±14.44 278.34—	0.21 ± 0.04 0.08 — 0.32	2.63 ± 1.46 0.71 — 4.50	-0.95 ± 0.89 -3.20 — 0.21-2.09± 1.74 -5.30—

Formatted: Justified, Tab stops: 0.77  
cm, Centered

					<del>366.70</del>			<del>0.25</del>
	Queen Maud	6192	6.72 ±	19.47 ±	<del>369.83 ± 11.04</del>	0.26 ± 0.07	2.60 ± 1.44	<del>-0.75 ± 0.62</del>
	Gulf		1.29	1.79	<del>327.32 -</del>	0.11 - 0.52	0.10 -	<del>-3.41 -</del>
			2.86 -	13.07 -	<del>404.64327.94</del>		5.87	<del>0.10-1.79±</del>
			8.81	24.54	<del>± 8.02</del>			<del>1.40</del>
					<del>291.33 -</del>			<del>-6.20 -</del>
					<del>362.30</del>			<del>0.02</del>
	Average all	11058	6.96 ±	20.12 ±	<del>373.37 ± 18.75</del>	0.24 ± 0.07	3.13 ± 1.96	<del>-0.57 ± 0.69</del>
			1.16	1.93	<del>308.66 -</del>	0.08 - 0.52	0.10 -	<del>-3.41 -</del>
			2.86 -	12.23 -	<del>427.40330.71</del>		7.47	<del>2.35-2.08±</del>
			9.65	24.54	<del>± 15.15</del>			<del>1.65</del>
					<del>278.34 -</del>			<del>-7.11 -</del>
					<del>376.12</del>			<del>0.02</del>

#### 345 4. Discussion

Presented in the results above are the multiyear summertime  $p\text{CO}_2$  (sw) observations made on *RV Martin Bergmann*. These data reveal the spatial and inter-annual variability of  $p\text{CO}_2$  (sw) ~~near the beginning of~~ throughout the open-water season in the Kitikmeot Sea. To maximise the value of the  $p\text{CO}_2$  (sw) observations made on *RV Martin Bergmann* we will now present and discuss these new measurements alongside previous measurements and in the context of our current understanding of the carbonate system in the region.

##### 4.1 Local scale – comparisons with the ocean carbon observatories

The two local observatories, the ONC mooring in Cambridge Bay and the Qikirtaarjuk Island observatory (Figure 1), provide measurements throughout the year that are not readily possible with shipboard observations.  $p\text{CO}_2$  (sw) is directly measured on the ONC mooring, whereas  $p\text{CO}_2$  (sw) is calculated from the flux derived using measurements from the Qikirtaarjuk Island observatory eddy covariance “EC tower”. ~~By taking~~ Using the  $p\text{CO}_2$  (sw) observations from these two observatories alongside the new *RV Martin Bergmann* measurements ~~allows us to construct~~ enables we can create a multiyear timeline of  $p\text{CO}_2$  (sw) in the region ~~to be constructed~~ (Figure 5). It should be noted that the three measurement sources in Figure 5 are not co-located, the Qikirtaarjuk Island observatory on the Finlayson Islands is 35 km west of the ONC mooring (Figure 1) and the Bergmann measurements span a slightly wider area (Figure 2). (Duke et al., 2021) Despite the spatial disparity in these measurements, it should also be acknowledged that for calculations of global  $\text{CO}_2$  flux on a  $1^\circ \times$

1° grid, the majority of these measurements would fall within the same grid cell. It might be expected that on these sorts of spatial scales the measurements should agree close ~~to perfectly~~, but that is ~~not~~ not always the case (Figure 5).

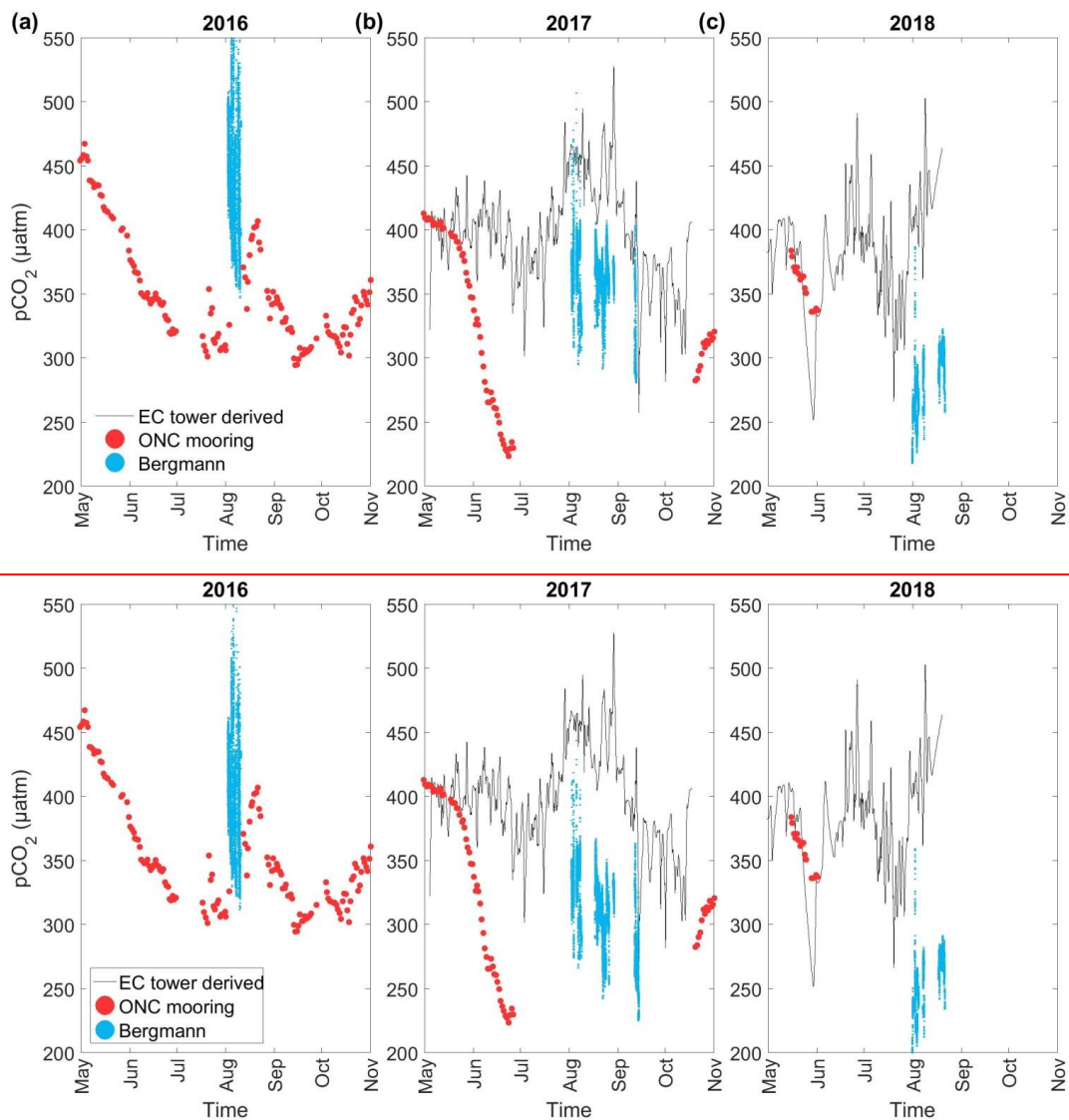


Figure 5: Surface  $p\text{CO}_2$  ( $\text{sw}$ ) from across the Kitikmeot Sea made in (a) 2016, (b) 2017 and (c) 2018.  $p\text{CO}_2$  ( $\text{sw}$ ) measurements from the ONC mooring are shown as red dots, all  $p\text{CO}_2$  ( $\text{sw}$ ) measurements from the RV *Martin Bergmann* are shown as blue dots and  $p\text{CO}_2$  ( $\text{sw}$ ) inferred from Eddy covariance at the Qikirtaarjuk Island observatory are shown as a black line.

365 The *RV Martin Bergmann*  $p\text{CO}_2$  (sw) data are ~~much~~ lower in 2017 (Figure 5b) and 2018 (Figure 5c) relative to the values  
predicted from the EC tower, even when measurements were made in the footprint of the EC tower. For example, from  
(18:30 – 23:10 on August 3<sup>rd</sup> August 2017,  $p\text{CO}_2$  (sw) from the tower was ~~414.675  $\mu\text{atm}$ 67~~ and from *RV Martin*  
*Bergmann* was ~~390.34424  $\mu\text{atm}$ 69~~; whereas, from 21:05:50– 06:40 on August 1<sup>st</sup> 2018,  $p\text{CO}_2$  (sw) from the tower was  
370 ~~408.699  $\mu\text{atm}$ 69~~ and from *RV Martin Bergmann* was ~~237.4062  $\mu\text{atm}$ 40~~). ~~The large differences between the methods can~~  
~~not be reasonably explained by changes due to SST~~ Accounting for a thermal skin temperature of 0.17°C in the *RV Martin*  
*Bergmann* ~~RV Bergmann~~ data only alters the  $p\text{CO}_2$  (sw) by about ~ 3  $\mu\text{atm}$  based on the 4.23% °C<sup>-1</sup> Takahashi et al. (1993)  
constant. ~~For the *RV Martin Bergmann*  $p\text{CO}_2$  (sw) to match values from the EC tower, based on the the 4.23% °C<sup>-1</sup> constant~~  
~~the SST at the surface would need to be 1.46 °C greater at the surface on August 3<sup>rd</sup> 2017 and 10.52°C greater at the surface~~  
375 ~~on August 1<sup>st</sup> 2018 than measured by *RV Martin Bergmann* at 1 m. Modelling results do not support the existence of~~  
~~temperature differences of the magnitude that can account for the  $p\text{CO}_2$  (sw) difference on August 3<sup>rd</sup> 2017 (Xu et al., 2021).~~  
~~It is possible that the SST measured from the 13 m mooring which is used to calculate  $p\text{CO}_2$  is not representative of the~~  
~~surface interface, which would bias the schmidt number and  $k_0$  used in the calculation of  $p\text{CO}_2$  (sw) from the tower; yet, even~~  
~~if this were the case, the magnitude of the impact can not explain the larger  $p\text{CO}_2$  (sw) differences between the methods (146~~  
 ~~$\mu\text{atm}$ ). Even though the *RV Martin Bergmann* measurements are being made close to the surface (at a depth of 1 m), the~~  
380 ~~however~~ ~~It is possible that the measured surface, which would be biased in our calculations; yet, (XX  $\mu\text{atm}$ ) as this would~~  
~~require (Xu et al., 2021) an extremely large temperature gradient – 5–10 °C between the *RV Martin Bergmann* SST at 1 m and~~  
~~SST at the interface. The most likely explanation for the differences in  $p\text{CO}_2$  (sw) between the two methods is that even~~  
~~though the *RV Martin Bergmann* measurements are being made close to the surface (at a depth of 1 m), surface stratification~~  
~~in the surface this upper meter is driving the differences being observed.~~ The impact of surface stratification on  $p\text{CO}_2$  (sw) has  
385 been observed elsewhere in the Arctic (Ahmed et al., 2020; Dong et al., 2021b) including for cases where differences can be  
up to 200  $\mu\text{atm}$  (Miller et al., 2018). Surface stratification in the Kitikmeot Sea is caused by melting of first-year sea ice and  
the large freshwater input by rivers (~~which rivers alone can alone~~ contribute an estimated 70 cm of freshwater to the surface  
annually); (Williams et al., 2018). The fact that the EC tower  $p\text{CO}_2$  (sw) was higher than the *RV Martin Bergmann*  $p\text{CO}_2$  (sw)  
would suggest that this is due to river induced stratification, as ~~river~~ Arctic riverine water is ~~often typically~~ higher in  $p\text{CO}_2$   
390 (sw) (Cai et al., 2010), ~~indeed this was true between the 30<sup>th</sup> June and 2<sup>nd</sup> July 2017 for Freshwater Creek (Manning et al.,~~  
~~2020) (Kljun et al., 2015).~~ Interestingly, the predicted  $p\text{CO}_2$  (sw) from the EC tower ~~shows show~~ a peak in early August 2017  
and a downwards trend through to the end of August, something that is also seen in the ~~ship ship~~-based  $p\text{CO}_2$  (sw)  
observations (Figure 5b). Similarly, the predicted  $p\text{CO}_2$  (sw) from the EC tower increases in August 2018 at a similar rate to  
the increase seen in the shipboard  $p\text{CO}_2$  (sw) observations (2.22  $\mu\text{atm d}^{-1}$ ) (Figure 5c). The fact that similar trends can be  
395 observed in the *RV Martin Bergmann* and the EC tower  $p\text{CO}_2$  (sw) does suggest that seasonal trends in the region are  
detectable with both methods. ~~However, the general~~ The disagreement between the *RV Martin Bergmann* measurements  
and those from the EC tower highlights the need for year-round  $p\text{CO}_2$  (sw) observations in the flux footprint of the EC tower.

Formatted: Superscript

Formatted: Superscript



Additionally, interfacial  $p\text{CO}_2$  (sw) measurements and vertical profiles may help reconcile the observed disparities seen between the two measurement sources of data.

400

~~On the other hand, there is good agreement in the  $p\text{CO}_2$  (sw) values between the EC tower and the ONC mooring in May, June, and October 2017 (average  $p\text{CO}_2$  (sw) EC tower for October 11<sup>th</sup> to 14<sup>th</sup> is 320  $\mu\text{atm}$  and is 311 for October 24<sup>th</sup> to 30<sup>th</sup>) (Figure 5b) and in May and June 2018 (Figure 5c). The breakdown of stratification at the end of the ice-free summer period and over the winter (Xu et al., 2021) may explain the good agreement between the EC tower and the ONC mooring at these times. In June 2017, the two systems diverge. Specifically, the  $p\text{CO}_2$  (sw) at the ONC mooring decreases due to a spring bloom (Duke et al., 2021), whereas  $p\text{CO}_2$  (sw) from the EC tower is not impacted, as does not. As the bloom in Cambridge Bay is caused by wastewater discharge (Back et al., 2021) it might be expected that this signal would not be detectable at the EC tower.~~

405

410

~~There appears to be ~~an~~ some agreement between the *RV Martin Bergmann* collected data and the ONC mooring in the summer of 2016. Unfortunately, the servicing period of the ONC mooring overlapped with the *RV Martin Bergmann* cruise dates meaning there was no period of direct data overlap between the two data sets. The four periods when the *RV Martin Bergmann* was moored up within 0.5 km of the mooring on 05:20–11:10 5<sup>th</sup> August 2016, 05:40–01:20 7/8<sup>th</sup> August 2016, 08:20–14:30 9<sup>th</sup> August 2016, 00:50–21:40 10<sup>th</sup> August 2016 the average  $p\text{CO}_2$  (sw) values were ~~433, 392, 58, 421, 384, 33, 406, 365, 85~~ and ~~370, 02, 406~~  $\mu\text{atm}$  respectively.  $p\text{CO}_2$  (sw) at the ONC mooring on 10:00 3<sup>rd</sup> August was 326  $\mu\text{atm}$  and on 12:40 12<sup>th</sup> August was 371  $\mu\text{atm}$ . Disagreement between the ONC mooring and the *RV Martin Bergmann* here may be due to the different intake depths of the two systems. Stratification may mean the ONC mooring is not always representative of  $p\text{CO}_2$  (sw) closer to the air-sea interface, especially during parts of ice free period of the year; however, CTD profiles from 2018 do indicate there is stratification in the surface 10 m in the summer (Back et al., 2021). The spring 2016 measurements from the ONC mooring show that  $p\text{CO}_2$  (sw) was high in the spring leading into the summer field season, and the trend towards increasing  $p\text{CO}_2$  (sw) due to warming is captured in August 2016 by both the ONC mooring and the *RV Martin Bergmann* observations.~~

415

420

425

Combining the data sources in this way highlights the value of having these different observatories to look at multiyear changes. The observatories provide context to the variability in the summertime  $p\text{CO}_2$  (sw) measurements from local ships. The patchiness/intermittence of the measurements from the ONC mooring and the Qikirtaarjuk Island observatory reflects the challenges in making these novel measurements in an extreme environment. Knowledge about how to run them/operate both observatories and prevent instrument outages means that future measurements will build towards much needed continuous and complementary multiyear datasets.

#### 430 4.2 Regional scales – spatial variability in the underway data

Focusing back on the *RV Martin Bergmann* data, there is clear evidence of spatial regional variability in the underway data.  $p\text{CO}_2$  (sw) was typically lower by  $\sim 20$ – $40$   $\mu\text{atm}$  in the small bays (Cambridge Bay, and Wellington Bay) and larger inlets surveyed (Bathurst Inlet, ~~Chantry~~Chantry Inlet) compared to the central channel (e.g., Dease Strait West, the Finlayson Islands, and Queen Maud Gulf) (Table 1). The reason for relatively lower  $p\text{CO}_2$  (sw) in the Bays and Inlets is not readily apparent. ~~For this trend to be driven by temperature, Using the 4.23 % °C<sup>-1</sup> constant from Takahashi et al. (1993) it is possible to test whether the pattern of lower  $p\text{CO}_2$  (sw) in the Bays and Inlets was driven by temperature, for a representative 360  $\mu\text{atm}$  value for  $p\text{CO}_2$  (sw) to be  $\sim 20$ – $40$   $\mu\text{atm}$  lower it would need to be between 1.35 and 2.78 °C colder the bays and inlets would need to be  $\sim 2$ °C colder, which was not observed. Rather than being colder, In fact,~~ many of these regions, such as Bathurst Inlet, were warmer, ~~and which would usually based on the Takahashi et al. (1993) constant, would thus have a predicted~~ predict higher  $p\text{CO}_2$  (sw).—Although the fluorescence sensor was not ~~robustly~~ calibrated against *in situ* measurements, the— fluorescence signal was consistent with previous measurements that showed the region to have widespread low primary production at the surface (Martin et al., 2013). ~~In spite of the lack of Even though these regions did not have consistently higher surface chlorophyll-a concentrations, biological production at depth can-not be ruled out as an explanation for lower  $p\text{CO}_2$  (sw) in the bays. For example, wastewater discharge has been shown to cause a deep (20 – 30 m) chlorophyll bloom in Cambridge Bay (Back et al., 2021). A large under ice (Arrigo et al., 2012; Mundy et al., 2009) or ice edge (Perrette et al., 2011) phytoplankton bloom earlier could also explain lower values in the season could also explain lower summertime  $p\text{CO}_2$  (sw) values in these bays and inlets that persists into summer.~~—It is also possible that these regional differences are driven by regional freshwater inputs; all four identified regions are fed by rivers and there are sharp salinity transitions of  $\sim 5$  that point to the existence of mixing and fronts (Figure 4c). Rivers are typically thought to be highly ~~oversaturated-supersaturated~~ in  $p\text{CO}_2$  (sw) in the Arctic due to organic matter breakdown (Teodoru et al., 2009), ~~potentially contributing to –so it might be expected that there would be higher  $p\text{CO}_2$  (sw) in these bays and inlets. However, whilst the freshwater local rivers are high in  $p\text{CO}_2$  (sw) (Manning et al., 2020), they are typically unbuffered and thus have much lower DIC relative to seawater. Whilst the average values for riverine TA (565  $\mu\text{mol kg}^{-1}$ ) and DIC (533  $\mu\text{mol kg}^{-1}$ ) in the CAA are low, maximum measured values for TA (2,272  $\mu\text{mol kg}^{-1}$ ) and DIC (2,252  $\mu\text{mol kg}^{-1}$ ) values can be as high or higher than in seawater, depending on the bedrock type underlying the drainage basin –(Brown et al., 2020). Dilution by low  $p\text{CO}_2$  (sw) ice meltwater does lower  $p\text{CO}_2$  (sw) (Cai et al., 2010; Meire et al., 2015), so it may be that, a greater impact of sea ice meltwater in these bays and inlets may be contributing to the lower observed  $p\text{CO}_2$  (sw).~~

The ONC mooring is located in Cambridge Bay in shallow water (~~sensor depth 79~~ m), at this depth the mooring is not impacted by the Freshwater Creek plume ~~which is detectable at  $< 2$  m~~ (Duke et al., 2021; Manning et al., 2020). It is still unclear how much of an impact being located in the ~~isolated~~-Bay has on the representativeness of these measurements for the Kitikmeot region. As the *RV Martin Bergmann* travelled into and out of the Bay multiple times during the four years of

observations, differences in  $p\text{CO}_2(\text{sw})$  measured in the Bay and outside the Bay may help identify whether the ONC mooring site is representative of the region as a whole. All transects into and out of Cambridge Bay are shown in Figure 6. Two sub-  
465 | regions are designated, inside the Bay and outside the Bay, [here](#)  $p\text{CO}_2(\text{sw})$  from the *RV Martin Bergmann* was averaged every  
two days for which there ~~was~~ were data available (Table 2). [As seen in Table 2](#),  $p\text{CO}_2(\text{sw})$  was ~~largely~~ similar (typically <  
 ~~$\pm 15 \mu\text{atm}$~~ ) inside and outside of the bay ~~with  $p\text{CO}_2(\text{sw})$  typically  $< \pm 12 \mu\text{atm}$~~ . On ~~the 17<sup>th</sup>~~-August ~~17<sup>th</sup>~~, 2017,  $p\text{CO}_2(\text{sw})$  was  
much higher (~~39.6~~ ~~33.29~~  $\mu\text{atm}$ ) in the Bay. ~~As~~ ~~as~~ measurements are similar before (8<sup>th</sup>/9<sup>th</sup>) and after (19<sup>th</sup>/20<sup>th</sup>) ~~the 17<sup>th</sup>~~  
470 | ~~August~~, it would appear that this difference is caused by ~~this would point to this being due to a process something~~ only  
~~occurring happening~~ in the Bay; possibly [related to](#) the river plume. Overall, the agreement between the measurements inside  
and outside of the Bay is encouraging and suggests that  $p\text{CO}_2(\text{sw})$  in Cambridge Bay, at least broadly agrees with that in the  
main Channel. Without more information, it is difficult to conclude whether the mooring is truly representative of the wider  
Kitikmeot Sea.

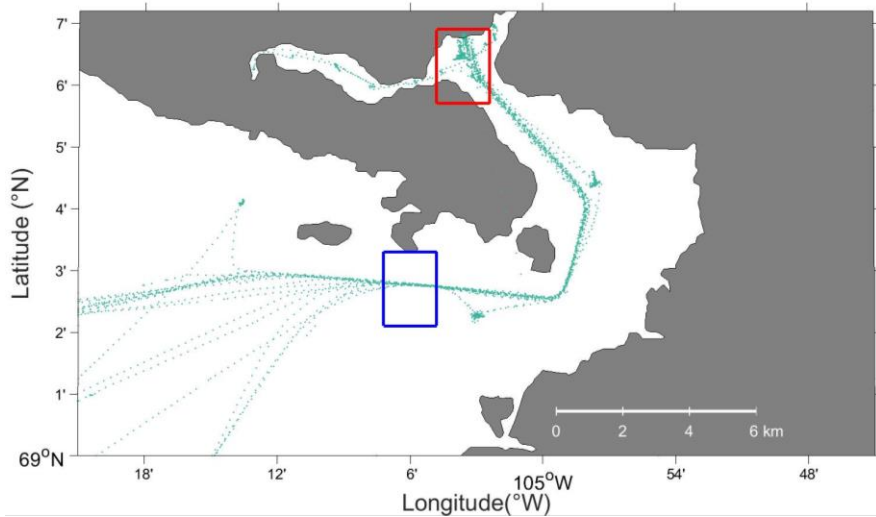
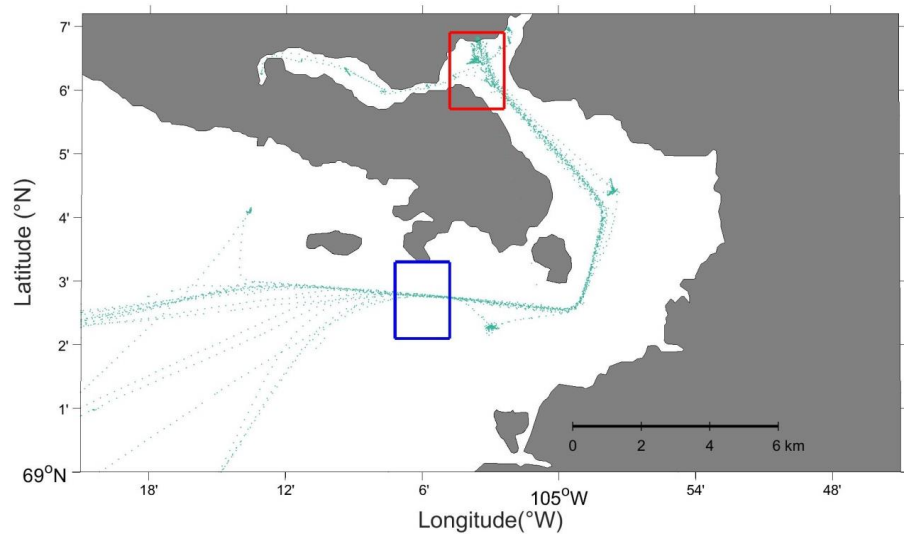


Figure 6: Zoomed in view showing the location of all the  $p\text{CO}_2$  (sw) transects (green) measured in and out of Cambridge Bay during the four years of transects. The regions used to define inside the Bay and outside the Bay are shown by a red and blue box respectively.

Table 2: Average  $p\text{CO}_2$  (sw) measured by the *RV Martin Bergmann* inside and outside of Cambridge Bay.

Date	$p\text{CO}_2$ (sw)	$p\text{CO}_2$ (sw)	$p\text{CO}_2$ (sw)
------	---------------------	---------------------	---------------------

	inside Cambridge Bay	outside Cambridge Bay	difference (inside Bay –outside Bay)
5 <sup>th</sup> August 2016	<del>405482.58</del>	<del>408.050.9</del>	<del>-2.231.6</del>
7 <sup>th</sup> - 8 <sup>th</sup> August 2016	<del>424468.2</del>	<del>415456.1.5</del>	<del>8.712.1</del>
9 <sup>th</sup> - 10 <sup>th</sup> August 2016	<del>423467.41</del>	<del>45712.73</del>	<del>40.89.7</del>
4 <sup>th</sup> - 5 <sup>th</sup> August 2017	<del>339.175.1</del>	<del>335.571.0</del>	<del>4.13.6</del>
6 <sup>th</sup> - 7 <sup>th</sup> August 2017	<del>340.074.2</del>	<del>335.470.2</del>	<del>4.06</del>
8 <sup>th</sup> - 9 <sup>th</sup> August 2017	<del>324.756.0</del>	<del>325.062.1</del>	<del>-0.36.1</del>
17 <sup>th</sup> August 2017	<del>381.5420.9</del>	<del>348.281.3</del>	<del>33.39.6</del>
19 <sup>th</sup> - 20 <sup>th</sup> August 2017	<del>334.271.2</del>	<del>337.574.8</del>	<del>-3.36</del>
29 <sup>th</sup> August 2017	<del>339.476.7</del>	<del>339.781.0</del>	<del>-40.3</del>
31 <sup>st</sup> July - 1 <sup>st</sup> August 2018	<del>221.5496.5</del>	<del>231.306.2</del>	<del>-9.87</del>
2 <sup>nd</sup> - 3 <sup>rd</sup> August 2018	<del>251.929.5</del>	<del>246.120.8</del>	<del>5.88.7</del>
8 <sup>th</sup> August 2018	<del>219.2494.6</del>	<del>221.5496.0</del>	<del>-2.31.4</del>
9 <sup>th</sup> August 2019	<del>280.8311.8</del>	<del>292.5326.7</del>	<del>-14.944.7</del>
18 <sup>th</sup> - 19 <sup>th</sup> August 2019	<del>360.321.4</del>	<del>364.027.3</del>	<del>-3.75.9</del>
21 <sup>st</sup> August 2019	<del>345.107.7</del>	<del>348.244.8</del>	<del>-34.1</del>

475

#### 4.3 Interannual variability and large scale seasonal trends

We have identified local scale differences between the  $p\text{CO}_2$  (sw) values from the *RV Martin Bergmann* and the ONC and the Qikirtaarjuk Island observatories and regional scales differences between the bays and inlets and the main channel.

However, large differences in the *RV Martin Bergmann*  $p\text{CO}_2$  (sw) values occurred between years. The measurement start date of all four cruises spanned a very short window of 10 days (2<sup>nd</sup> August 2016, 2<sup>nd</sup> August 2017, 31<sup>st</sup> July 2018, 9<sup>th</sup> August 2019). Ahmed et al. (2019) have established the importance of the timing of sea ice breakup on  $p\text{CO}_2$  (sw) values in the CAA. During our study, ice breakup began (4<sup>th</sup> July 2016, 22<sup>nd</sup> June 2017, 15<sup>th</sup> July 2018, 14<sup>th</sup> July 2019) ~2–6 weeks before the start of these cruises (4<sup>th</sup> July 2016, 22<sup>nd</sup> June 2017, 15<sup>th</sup> July 2018, 14<sup>th</sup> July 2019), which we interpret as exerting one of the main controls of the inter-annual variability in the *RV Martin*

485 *Bergmann*  $p\text{CO}_2$  (sw) data.

The very low  $p\text{CO}_2(\text{sw})$  values (~~261-289~~  $\mu\text{atm}$ ) observed in 2018 (Table 1) could be caused by a combination of low  $\text{SST}_{(1\text{m})}$ , springtime  $\text{CO}_2$  depletion by primary production and recent dilution by sea ice melt (Else et al., 2012; Ahmed et al., 2021; Geilfus et al., 2015) or river runoff ~~at where salinities are >20~~ (Cai et al., 2010). ~~yet~~ Without identifying clear ~~chemical signatures that can be attributed to each process it is difficult to~~ we cannot say with certainty which of these processes was most important in producing these low  $p\text{CO}_2(\text{sw})$  values. As the ice breakup was late in 2018 (resulting in samples collected shortly after breakup), it can be assumed that surface ocean  $\text{CO}_2$  exchange with the atmosphere was limited by the ice cover until just before these measurements were made, as sea ice is essentially impermeable to gases (Loose et al., 2011; Butterworth and Else, 2018). Additionally, ~~the presence of sea ice through to the end of July~~ ~~over in 2018 prevented warming of~~ ~~meant there was far less warming of the~~ surface seawater ~~as~~ (average  $\text{SST}_{(1\text{m})}$  ~~was~~  $4.32^\circ\text{C}$  ~~low in 2018~~), ~~this explanation rules out surface cooling lowering~~  $\text{SST}_{(1\text{m})}$  and thus  $p\text{CO}_2(\text{sw})$ . Light penetrating through sea ice between ~~March and June~~ could have driven primary production below and within the ice (Else et al., 2019). Indeed, an increase in under-ice chlorophyll *a* concentration together with a draw-down of surface nutrients between April to June 2018 ~~indicate supported~~ under-ice phytoplankton production during this period (Dalman et al., 2019). However, ~~chlorophyll *a* concentrations did not exceed  $0.6 \mu\text{g L}^{-1}$ , as production is limited by surface nutrient availability in the region (Back et al., 2021).~~ It is likely that the melting sea ice stratified the surface and diluted surface  $p\text{CO}_2(\text{sw})$  as has been observed in other parts of the Arctic (Miller et al., 2018; Ahmed et al., 2020); low ~~surface ocean~~ salinity values in the first weeks of the survey support this. Measurements several weeks into the 2018 cruise show that  $p\text{CO}_2(\text{sw})$  increased quickly in the following weeks ~~(to ~~XXX~~  $\sim 300 \mu\text{atm}$ ),~~ likely due to a combination of air-sea exchange and the observed surface warming. Interestingly, Ahmed et al. (2019) did not observe  $p\text{CO}_2(\text{sw})$  values below  $300 \mu\text{atm}$  at any point during the five years of passing through the Kitikmeot Sea. Therefore, 2018 could be an anomalously low year for  $p\text{CO}_2(\text{sw})$ , or the discrepancy could highlight the fact that (Ahmed et al., 2019) did not make any measurements immediately after ~~sea ice breakup in this region in the region.~~ Furthermore, the discrepancy could be influenced by the difference in sampling depth of the two  $p\text{CO}_2$  systems between the *CCGS Amundsen* (7 m) and *RV Martin Bergmann* (1 m). The best way to assess the impact of the sampling depth would be to take simultaneous measurements via the ships intake and at the interface as in Ho and Schanze (2020).

The processes driving the changes in  $p\text{CO}_2(\text{sw})$  ~~that have been discussed above can be partially quantified using back of the envelope calculations with several assumptions. The individual impact on  $p\text{CO}_2(\text{sw})$  of dilution by melting sea ice, air-sea gas exchange, net community production (NCP) and warming of seawater are explored across the region for the month of August in 2018.~~

~~Firstly, the impact of dilution by sea ice melt can be tested by assuming conservative mixing of TA, DIC, and salinity as in (Meire et al., 2015). For the seawater mixing endmember, surface TA ( $2034.43 \mu\text{mol kg}^{-1}$ ) and DIC ( $1958.82 \mu\text{mol kg}^{-1}$ ), SST ( $-1.38^\circ\text{C}$ ) and salinity (28.64) are taken from seawater bottle data on the 18<sup>th</sup> June 2018 (Duke et al., 2021) alongside surface silicate ( $4 \mu\text{mol L}^{-1}$ ) and phosphate ( $0.5 \mu\text{mol L}^{-1}$ ) from 2018 (Back et al., 2021). Average values from spring 2019~~

for TA (356.60  $\mu\text{mol kg}^{-1}$ ), DIC (340.24  $\mu\text{mol kg}^{-1}$ ) and salinity (4.56) in first year sea ice are used for the sea ice mixing end member (Else et al., 2022). Taking a sea ice thickness of 1.8 m and assuming water expands 10% when it freezes to form sea ice, would suggest melting all the sea ice would add 1.64 m of water, to reach the final salinity of 24.82 (the average recorded value from the *RV Martin Bergmann* measurements) with conservation of salinity would require this freshwater to mix with 8.68 m of seawater. The ratio of these two depths can then be used to provide the predicted TA (1768.26  $\mu\text{mol kg}^{-1}$ ), and DIC (1702.05  $\mu\text{mol kg}^{-1}$ ), for the seawater at a salinity of 24.82. Using CO2SYS (Lewis et al., 1998; Van Heuven et al., 2011) the calculated  $p\text{CO}_{2(\text{sw})}$  value for the initial seawater conditions is 369  $\mu\text{atm}$  and after the melting of sea ice  $p\text{CO}_{2(\text{sw})}$  is 302  $\mu\text{atm}$ , under constant temperature. The dissociation constants of carbonic acid used in the CO2SYS calculations were those by Mehrbach et al. (1973) refit by Dickson and Millero (1987) and the  $\text{HSO}_4^-$  dissociation constants from (Dickson, 1990). For these calculations temperature was kept constant. As the average measured  $p\text{CO}_2$  was 289  $\mu\text{atm}$  in 2018, sea ice melt and conservative mixing of seawater can account for the majority (66.75  $\mu\text{atm}$ ) of the total change in  $p\text{CO}_2$  (80  $\mu\text{atm}$ ) from the initial seawater conditions in 2018.

Secondly, using the same approach as DeGrandpre et al. (2020) an estimate of the individual and combined impact of air-sea exchange and NCP on  $p\text{CO}_{2(\text{sw})}$  can be made using a simple model with the following assumptions: taking the average flux from the 2018 cruise of  $-16.79 \text{ mmol m}^{-2} \text{ d}^{-1}$ , a 40 m mixed layer depth for Dease Strait (Xu et al., 2021), with a density of ( $996.49 \text{ kg m}^{-3}$ ) from SST ( $-1.38^\circ\text{C}$ ) and salinity (28.64), an upper estimate of NCP ( $6.63 \text{ g C m}^{-2}$ ) which is the average integrated rate for Cambridge Bay during the open water season of 2018 (Back et al., 2021). With this configuration a change in DIC ( $+0.0176 \mu\text{mol kg}^{-1} \text{ hr}^{-1}$ ) due to air-sea exchange and NCP ( $-0.003 \mu\text{mol kg}^{-1} \text{ hr}^{-1}$ ) can be calculated. Taking the combined change in DIC ( $+0.0142 \mu\text{mol kg}^{-1} \text{ hr}^{-1}$ ) and substituting it into CO2SYS (Van Heuven et al., 2011; Lewis et al., 1998) with the same initial TA, DIC, silicate and phosphate concentrations as on the 18<sup>th</sup> June 2018, produces a  $p\text{CO}_{2(\text{sw})}$  change of 0.0459  $\mu\text{atm hr}^{-1}$  for one time step. Scaling this DIC change for the month of August, with no other changes in the system, would increase  $p\text{CO}_{2(\text{sw})}$  by 36.31  $\mu\text{atm}$  (with NCP component reducing  $p\text{CO}_{2(\text{sw})}$  by 9.4  $\mu\text{atm}$  and air-sea exchange component increasing  $p\text{CO}_{2(\text{sw})}$  by 47.34  $\mu\text{atm}$ ).

~~we can derive. Here we make for the 2018 cruise: air-sea  $\text{CO}_2$  determined and. From this we can calculate the S due to air-sea exchange and NCP (Van Heuven et al., 2011; Lewis et al., 1998).~~

Thirdly, using the  $4.23 \% \text{ } ^\circ\text{C}^{-1}$  Takahashi et al. (1993) constant, the impact of the  $0.078 \text{ } ^\circ\text{C d}^{-1}$  warming trend on  $p\text{CO}_{2(\text{sw})}$  can be calculated for the 22 day period from July 31<sup>st</sup> to 22<sup>nd</sup> August 2018. Using the average  $p\text{CO}_{2(\text{sw})}$  value of 289  $\mu\text{atm}$  and SST<sub>(1m)</sub> of  $4.32 \text{ } ^\circ\text{C}$ , an increase in temperature of  $1.72 \text{ } ^\circ\text{C}$  of warming would predict a  $p\text{CO}_{2(\text{sw})}$  of 310  $\mu\text{atm}$ . This increase of 21.78  $\mu\text{atm}$  is less than the 22 day increase of 48.84  $\mu\text{atm}$  based on the  $2.22 \mu\text{atm d}^{-1}$  trend in the 2018 *RV Martin Bergmann* data. From this, the impact of warming can account for just under half of the change in  $p\text{CO}_{2(\text{sw})}$ , the rest of the increase in  $p\text{CO}_{2(\text{sw})}$  could be due to air-sea gas exchange.

Formatted: Superscript

Formatted: Subscript

Formatted: Subscript

Formatted: Subscript

Formatted: Subscript

Formatted: Subscript

555 To summarise, modelling the processes impacting  $p\text{CO}_{2-(\text{sw})}$  can account for much of the observed changes in  $p\text{CO}_{2-(\text{sw})}$  in  
2018. Sea ice melt can account for a 66.75  $\mu\text{atm}$  decrease in  $p\text{CO}_{2-(\text{sw})}$  equivalent to 83 % of the observed change. The  
warming of seawater by 1.72 °C in the first 22 days of August would increase  $p\text{CO}_{2-(\text{sw})}$  by 21.78  $\mu\text{atm}$ . Air sea gas exchange  
can account for a 47.34  $\mu\text{atm}$  increase in  $p\text{CO}_{2-(\text{sw})}$  in the month of August (34.72  $\mu\text{atm}$  if scaled to the first 22 days). NCP  
560 can account for a 9.4  $\mu\text{atm}$  decrease in  $p\text{CO}_{2-(\text{sw})}$  in August (-6.7  $\mu\text{atm}$  if scaled to the first 22 days). The actual observed  
change in  $p\text{CO}_{2-(\text{sw})}$  in the first 22 days of August was 48.77  $\mu\text{atm}$  which is extremely close to the combined  $p\text{CO}_{2-(\text{sw})}$  change  
from these three processes 48.68  $\mu\text{atm}$ .

~~Whilst~~ Whilst not as heavily undersaturated as in 2018,  $p\text{CO}_{2(\text{sw})}$  was still ~~highly~~ undersaturated with respect to atmospheric  
values in both 2017 and 2019. In these two years, measurements were made ~4–8 weeks after sea ice breakup and  $p\text{CO}_{2(\text{sw})}$   
565 values were in the ~~~300-350~~ 350-390  $\mu\text{atm}$  range. Having been ice free for longer,  $\text{SST}_{(1\text{m})}$  was 3–4 °C warmer in 2017 and  
2019 which accounts for much of the  $p\text{CO}_{2(\text{sw})}$  difference relative to 2018. Warming-Increased  $\text{SST}_{(1\text{m})}$  in 2017 and 2019 and  
a gradual increase in surface salinity in 2019 ~~mirror~~ the seasonal trends seen in Ahmed et al. (2019) where the CAA  
becomes saltier and warmer over the summer. The 2017 and 2019  $p\text{CO}_{2(\text{sw})}$  values are ~~lower than~~ similar but still slightly  
lower than the the majority of  $p\text{CO}_{2(\text{sw})}$  values observed in Coronation Gulf by Ahmed et al. (2019) which again likely  
570 reflects the slightly earlier sampling period of this study, where undersaturated surface waters that are recently ice-free  
~~surface waters~~ have not had long to equilibrate with the atmosphere or warm up.

Measured  $p\text{CO}_{2(\text{sw})}$  was much higher in 2016 (445.08  $\mu\text{atm}$ ) compared to 2017 and 2019 around four weeks after sea ice  
breakup. Ahmed et al. (2019) also observed similar  $p\text{CO}_{2}$  ~~oversaturation-supersaturation~~ (464.5  $\mu\text{atm}$ ) in the region in 2016  
575 when they made their observations ~2 weeks later ~~than what we show here~~.  $p\text{CO}_{2(\text{sw})}$  ~~oversaturation-supersaturation~~ requires  
either the upwelling of high  $p\text{CO}_{2(\text{sw})}$  deep waters, net heterotrophy, or for  $p\text{CO}_{2(\text{sw})}$  to be close to equilibrium with the  
atmosphere and then for the seawater to subsequently heat warm up (Chierici et al., 2011). The most plausible and observable  
of these is the warming of the surface waters. However, if  $\text{SST}_{(1\text{m})}$  variability was the main factor controlling  $p\text{CO}_{2(\text{sw})}$  i-  
it is not apparent why there would be ~~oversaturation-supersaturation~~ in 2016, but not in 2017 and 2019 which were both  
580 warmer years ~~if  $\text{SST}_{(1\text{m})}$  variability was the main factor controlling  $p\text{CO}_{2(\text{sw})}$~~ . The sea ice breakup time in 2016 was similar  
to both 2017 and 2019, suggesting that the timing of breakup was also not the only determining factor. We propose that t  
the high  $p\text{CO}_{2(\text{sw})}$  values observed in 2016 observed under similar conditions to both 2017 and 2019 may point to the importance  
of the surface  $p\text{CO}_{2(\text{sw})}$  values set value in the previous autumn and wintertime modulation of  $p\text{CO}_{2(\text{sw})}$ . To determine what  
585 processes are altering  $p\text{CO}_{2(\text{sw})}$  between summertime field seasons would require year round sampling or a ~~full~~  
biogeochemical model ~~would need to be~~ run over multiple years, which are outside of the scope of this paper.

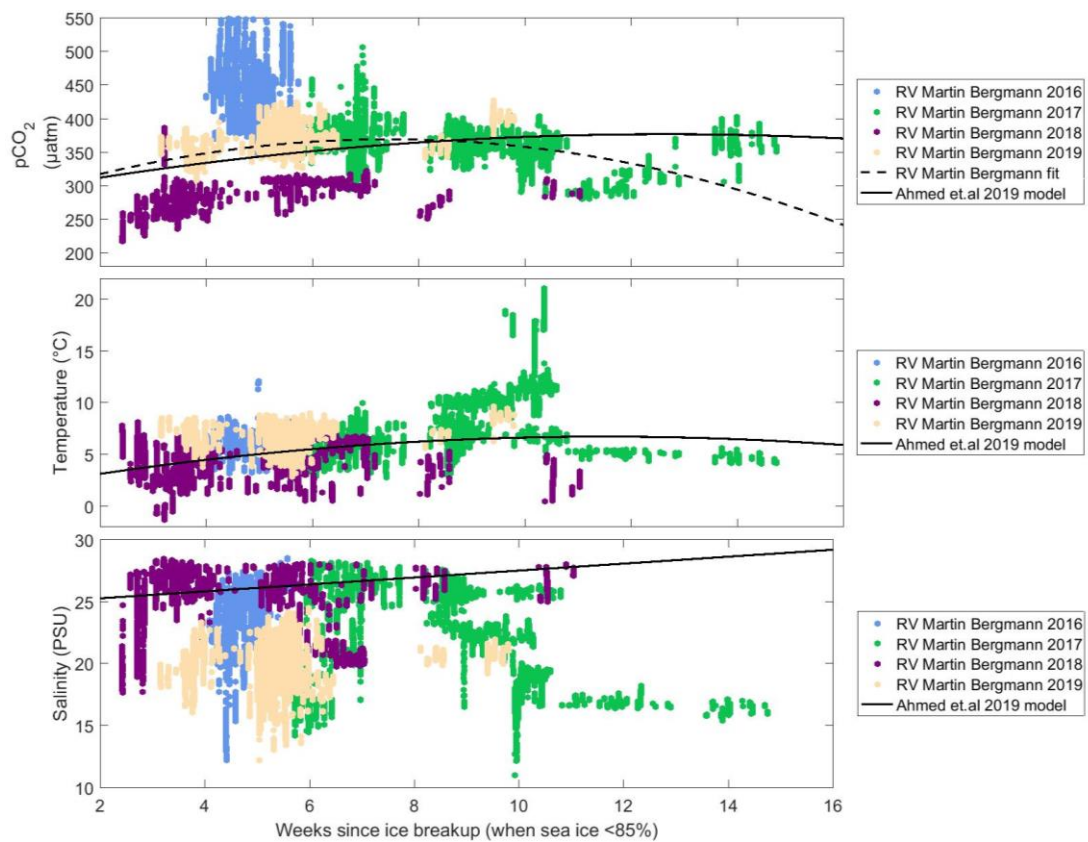
Clearly, many interacting processes are involved in determining surface ocean  $p\text{CO}_{2(\text{sw})}$  values in the Kitikmeot Sea, and as  
such, predicting surface ocean  $p\text{CO}_{2(\text{sw})}$  in this region is difficult. Ahmed et al. (2019) proposed a model for  $p\text{CO}_{2(\text{sw})}$  in the

Formatted: Font: Not Italic



CAA as a function of weeks since ice breakup, their model underestimated  $p\text{CO}_2_{(sw)}$  in the Kitikmeot Sea by  $\sim 26 \mu\text{atm}$  which they suggest may be due to the influence of rivers. Following their approach, the surface  $p\text{CO}_2_{(sw)}$ , SST, and salinity measurements from this study are presented as a function of time since ice melt (when sea ice concentration declines below 85%; Figure 7). The *RV Martin Bergmann* observations are ~~fairly-broadly~~ consistent with the general  $p\text{CO}_2$  model of Ahmed et al. (2019), where low  $p\text{CO}_2_{(sw)}$  values ( $\sim 300 \mu\text{atm}$ ) are seen shortly after sea melt and higher values ( ~~$\sim 300\text{--}300$~~   ~~$\text{--}$~~   ~~$350\text{--}350$~~   $\mu\text{atm}$ ) are seen in the following two months ~~that follow~~ after sea ice melt. However, the 2016  $p\text{CO}_2_{(sw)}$  values are much higher ~~(XX)~~ and the 2018 values are much lower ~~(YY)~~ than predicted by the model. The model is also not ~~able to a~~ good predictor of the observed salinity values in 2016 and 2019. The CAA flux estimate (Ahmed and Else, 2019) determined using the (Ahmed et al., 2019) model remains the best estimate for the region. However, the model is clearly unable to capture the full inter-annual variability in the *RV Martin Bergmann* observations. This could be because as a CAA wide model it is not tuned to the Kitikmeot Sea where freshwater inputs are greater. Fitting a quadratic equation to the *RV Martin Bergmann*  $p\text{CO}_2_{(sw)}$  observations produces the following equation:  $p\text{CO}_2_{(sw)} = -1.7452(X^2) + 26.0281(X) + 272.7442$  which can be used to model  $p\text{CO}_2_{(sw)}$ , where X is weeks since ice breakup. Both ~~models~~ predict very similar  $p\text{CO}_2_{(sw)}$  in the first seven weeks after sea ice breakup, the average difference between the models for this period is  $8.01 \mu\text{atm}$ . The models differ more after 7 weeks after sea ice breakup. At 14 weeks after sea ice breakup, the model of Ahmed et al. (2019) predicts a  $p\text{CO}_2_{(sw)}$  that is  $81.2 \mu\text{atm}$  higher than the model fit to the *RV Martin Bergmann*  $p\text{CO}_2_{(sw)}$  observations. Fundamentally, understanding the drivers of the large interannual variability in  $p\text{CO}_2_{(sw)}$  seen in the Kitikmeot Sea requires an understanding of the interconnected processes involved and their timing. The interannual variability SST<sub>(1m)</sub> and salinity are comparable to the modelling results of Xu et al. (2021), ~~by e.~~ Expanding ~~expanding~~ on that modelling work with a complex biogeochemical model that can incorporate all the known processes impacting  $p\text{CO}_2_{(sw)}$  ~~it~~ may make it ~~be~~ possible to accurately reproduce the  $p\text{CO}_2_{(sw)}$  observations in this region.

610



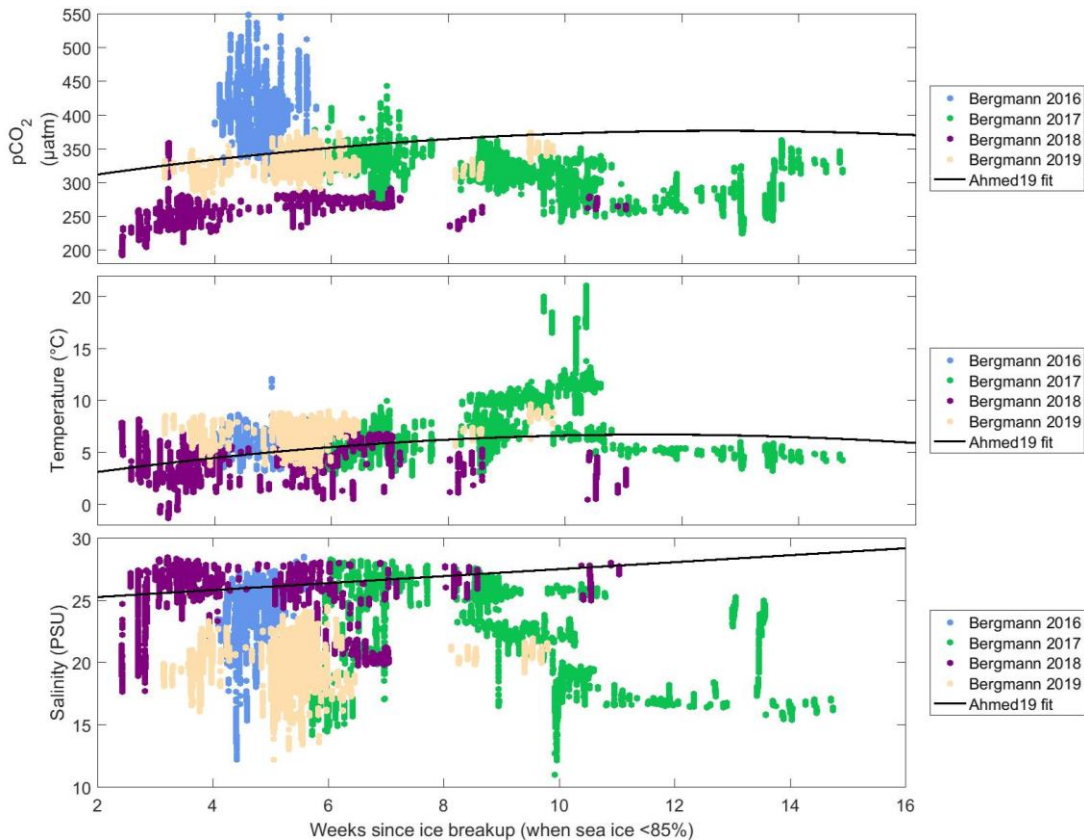


Figure 7: Surface (a)  $p\text{CO}_2$  (sw), (b) SST, and (c) salinity from the *RV Martin Bergmann* as a function of weeks of open water for years 2016 to 2019. A quadratic fit to the *RV Martin Bergmann*  $p\text{CO}_2$  (sw) data is shown as a dashed black line. Black curves represent the model output of Ahmed and Else (2019).

#### 4.4 The Kitikmeot Sea as a sink for atmospheric $p\text{CO}_2$

The *RV Martin Bergmann*  $p\text{CO}_2$  (sw) measurements indicate that the region is a  $\text{CO}_2$  sink in early August, most years (Table 1). At sea ice breakup, low- $\text{SST}_{(1\text{m})}$  values are low impacts increases solubility resulting in and there are large  $\Delta p\text{CO}_2$  gradients between the surface ocean and the atmosphere, these conditions persist for several weeks after sea ice breakup.

615 Warming of the surface ocean when  $p\text{CO}_2$  (sw) is slightly undersaturated is the likely cause of  $p\text{CO}_2$  (sw) oversaturation supersaturation in some years, resulting in the region becoming a net source once the saturation threshold is met later in the season. Decreasing  $\text{SST}_{(1\text{m})}$  at the end of the ice-free season lowers  $p\text{CO}_2$  (sw), producing a second period when there are larger  $\Delta p\text{CO}_2$  gradients between the ocean and the atmosphere, this is partially identifiable in the *RV Martin Bergmann*

Formatted: Subscript

620 ~~measurements from late in 2017. Whilst not demonstrable with the RV Martin Bergmann measurements, cooling decreased SST<sub>(1m)</sub> at the end of the ice free season should lower pCO<sub>2(sw)</sub>, thereby providing a second period when there are large ΔpCO<sub>2</sub> gradients between the ocean and the atmosphere.~~ The magnitude of the ΔpCO<sub>2</sub> and thus the size of the CO<sub>2</sub> sink throughout the summer, appears ~~to~~ not only to be driven by time since ice breakup, but also by the absolute surface ocean pCO<sub>2(sw)</sub> value at the time of ice breakup. Ahmed and Else (2019) used remote sensing products to identify this region as a net sink when the flux is integrated over the full ice-free period. ~~Our~~ Our measurements corroborate these findings.

625 The large variability in pCO<sub>2(sw)</sub> measured in the four years of observations highlights the fact that, in the Arctic, single cruises in only part of the ice-free season are likely not capturing the full seasonal variability in these regions. Many pCO<sub>2(sw)</sub> observations in the Arctic are temporally biased towards the middle of the ice-free season, when moving vessels through the Arctic Ocean is easiest. As these single cruises are the only measurements in many of these regions in databases like 630 SOCAT (Bakker et al., 2016), they could result in a biased regional flux estimates in these regions. In particular, it should be acknowledged that the majority of the CAA is not included in the state of the art observational based products (Landschützer et al., 2020).

## 5. Conclusions

635 The ONC mooring and EC tower both provide similar pCO<sub>2(sw)</sub> values in spring and autumn showing good agreement between the two platforms. Measured pCO<sub>2(sw)</sub> from the EC tower was ~~sometimes similar to much higher than~~ what was measured from the RV Martin Bergmann ~~whereas at other times it was much higher. but~~ Similar seasonal trends which are likely related to temperature were seen in pCO<sub>2(sw)</sub> from the EC tower and the RV Martin Bergmann both data sources which may be attributable to surface stratification caused by sea ice melt and riverine flows inputs. Comparing measurements collected by the RV Martin Bergmann in and out of Cambridge Bay indicates that Cambridge Bay surface ocean pCO<sub>2(sw)</sub> is 640 ~~not drastically different from similar to that in the main channel Dease Strait~~ in August. This may indicate that pCO<sub>2(sw)</sub> at the ONC mooring may be broadly representative of Dease Strait.

645 The Kitikmeot Sea was a CO<sub>2</sub> sink ~~from the atmosphere~~ or a very weak-weak CO<sub>2</sub> source over the summers of 2016 – 2019, consistent with previous measurements from Ahmed and Else (2019). The CO<sub>2</sub> sink was highly variable from year to year at the beginning of August (average observed fluxes of ~~+3.58, -2.96, -16.79 and -0.57~~ 0.41, -7.70, -21.26 and -2.08 mmol m<sup>-2</sup> d<sup>-1</sup> during the 2016, 2017, 2018, and 2019 cruises respectively) with average pCO<sub>2(sw)</sub> as low as ~~288.55 261.19 ± 19.70~~ μatm and as high as ~~445.08 403.65 ± 44.44~~ μatm. pCO<sub>2(sw)</sub> was much lower in 2018 due to the much lower SST<sub>(1m)</sub> that year. The magnitude of the air-water ΔpCO<sub>2</sub> throughout the summer appears to be controlled by the absolute pCO<sub>2(sw)</sub> value at the time of ice breakup. Low pCO<sub>2(sw)</sub> values increase in August due to exchange with the atmosphere and warming broadly 650 following the predicted trends using the model developed by Ahmed et al. (2019). In years where pCO<sub>2(sw)</sub> is high when ice

breakup occurs, warming can cause a period of slight  $p\text{CO}_2$  (sw) ~~oversaturation-supersaturation~~ in summer, in these situations the magnitude of this ~~oversaturation-supersaturation~~ is likely moderated by the ~~air-air~~-sea flux reducing  $p\text{CO}_2$  (sw).  $p\text{CO}_2$  (sw) was found to be ~20–40  $\mu\text{atm}$  lower in the Bays and Inlets that were surveyed; this could be driven by [increased](#) freshwater inputs into these isolated regions. Lower  $p\text{CO}_2$  in [the](#) bays and inlets would represent an observational bias in the CAA-wide surveys (Ahmed et al., 2019). [Local](#) freshwater fluxes into the southern CAA are much greater than elsewhere in the CAA, meaning that this bias might be more prominent in the Kitikmeot Sea. Further observations in these regions may complement the basin-level  $p\text{CO}_2$  mapping.

These findings provide a more nuanced picture of the considerable inter-annual variability in  $p\text{CO}_2$  (sw) observed during repeat cruises in the same region, underscoring how much may be missed by relying on data collected during one-off cruises along the ~~dynamic~~ Arctic coasts. [In particular,](#) ~~t~~he  $p\text{CO}_2$  (sw) at the time of ice melt is very important as it dictates the magnitude and direction of the flux for much of the ice-free period; ~~however,~~ ~~Aa~~-A better understanding of  $p\text{CO}_2$  (sw) through the ice covered period is needed to help unravel the seasonal and interannual variability.

## 6. Acknowledgements

Parts of this research were completed on or adjacent to Inuit Owned Lands under the authority of the Nunavut Land Claim Agreement, and the work was licensed by the Nunavut Research Institute. We thank the Ekaluktutiak Hunters and Trappers Organization and the community of Cambridge Bay for their hospitality and support of this project. Richard Sims was supported through the University of Calgary's Eyes High Postdoctoral fellowship program. This work was funded by The Marine Environmental Observation, Prediction and Response Network (MEOPAR, project number 1-02-02-004.1), The Kitikmeot Sea Science Study (K3S), [Fisheries and Oceans Canada, the Arctic Resrach Foundation](#), the Natural Sciences and Engineering Research Council of Canada (Discovery and Northern Research Supplement grants to B. Else, RGPIN-2015-04780), and the Canada Foundation for Innovation (John R. Edwards Leaders Fund grant to B. Else, 34814). Logistical support was provided by the Arctic Research Foundation. Samantha Jones, Stephen Gonski and Patrick Duke were supported by Polar Knowledge Canada through the Northern Scientific Training Program. We thank Polar Knowledge Canada and the Canadian High Arctic Research Station for their support and for providing accommodation and vehicles during field campaigns. Data from Ocean Networks Canada was accessed under their Creative Commons CC-BY 4.0 License. We thank the captain and crew of the *RV Martin Bergmann* for all their assistance. We also thank Shawn Marriott and Francis Emingak for all their assistance in the field, and Sophia Ahmed for her work on data interpretation.

## 7. Author Contributions

680 This manuscript was written by RPS, all co-authors made contributions to the final paper. BTGE installed the underway  
system at the start of each field season. The performance of the underway system was monitored by BTGE with help from  
SFJ, SFG, KAB, PJD and RPS. RPS organised and processed the data. RPS made the figures and interpreted the results and  
with support from MA and BTGE. BJB analysed the data from the EC tower and provided that data for this paper. PJD  
provided the data from the ONC mooring. BTGE, KAB, CJM and WJW ~~secured have been were~~ central in planning the  
685 cruise programme. BTGE oversaw completion of the work.

## 8. Data and code availability

The processed underway data from the *RV Martin Bergmann* which is the new data described in this paper is available in the  
supplement as .mat files. The raw and processed underway data from the *RV Martin Bergmann* data will also be available via  
Zenodo. The final processed data will also be submitted to the Surface Ocean Carbon Atlas (SOCAT). The wind data and  
690 inferred seawater  $p\text{CO}_2$  data from the EC tower are included in the supplement as .mat files. The ONC mooring data is freely  
available at <https://data.oceannetworks.ca/home>. The AMSR2 sea ice data [https://seaice.uni-  
bremen.de/data/amr2/asi\\_daygrid\\_swath/n3125/](https://seaice.uni-bremen.de/data/amr2/asi_daygrid_swath/n3125/) the NCEP winds  
<https://psl.noaa.gov/data/gridded/data.ncep.reanalysis2.html> and the atmospheric  $p\text{CO}_2$  data from Barrow  
[ftp://aftp.cmdl.noaa.gov/data/greenhouse\\_gases/co2/in-situ/surface/](ftp://aftp.cmdl.noaa.gov/data/greenhouse_gases/co2/in-situ/surface/) which were used in this paper are all freely available  
695 from their online repositories. Processing code and the code needed to reproduce the figures was written in Matlab 2016a.  
The code is provided in the supplement and is also available at [https://github.com/Richard-  
Sims/Sims\\_2022\\_Bergmann\\_pCO2](https://github.com/Richard-Sims/Sims_2022_Bergmann_pCO2).

## References

- Ahmed, M., Else, B., Burgers, T., and Papakyriakou, T.: Variability of surface water  $p\text{CO}_2$  in the Canadian Arctic  
700 Archipelago from 2010 to 2016, *Journal of Geophysical Research: Oceans*, 124, 1876-1896,  
<https://doi.org/10.1029/2018JC014639>, 2019.
- Ahmed, M., and Else, B. G.: The Ocean  $\text{CO}_2$  Sink in the Canadian Arctic Archipelago: A Present-Day Budget and Past  
Trends Due to Climate Change, *Geophysical research letters*, 46, 9777-9785, <https://doi.org/10.1029/2019GL083547>, 2019.
- 705 Ahmed, M. M., Else, B. G., Capelle, D., Miller, L. A., and Papakyriakou, T.: Underestimation of surface  $p\text{CO}_2$  and air-sea  
 $\text{CO}_2$  fluxes due to freshwater stratification in an Arctic shelf sea, Hudson Bay, *Elementa: Science of the Anthropocene*, 8,  
084, <https://doi.org/10.1525/elementa.084>, 2020.
- Ahmed, M. M., Else, B. G., Butterworth, B., Capelle, D. W., Guéguen, C., Miller, L. A., Meilleur, C., and Papakyriakou, T.:  
Widespread surface water  $p\text{CO}_2$  undersaturation during ice-melt season in an Arctic continental shelf sea (Hudson Bay,  
Canada), *Elem Sci Anth*, 9, 00130, <https://doi.org/10.1525/elementa.2020.00130>, 2021.
- 710 Arrigo, K. R., Perovich, D. K., Pickart, R. S., Brown, Z. W., Van Dijken, G. L., Lowry, K. E., Mills, M. M., Palmer, M. A.,  
Balch, W. M., and Bahr, F.: Massive phytoplankton blooms under Arctic sea ice, *Science*, 336, 1408-1408, DOI:  
10.1126/science.1215065, 2012.

- Back, D.-Y., Ha, S.-Y., Else, B., Hanson, M., Jones, S. F., Shin, K.-H., Tatarek, A., Wiktor, J. M., Cicek, N., and Alam, S.: On the impact of wastewater effluent on phytoplankton in the Arctic coastal zone: a case study in the Kitikmeot Sea of the Canadian Arctic, *Science of The Total Environment*, 764, 143861, <https://doi.org/10.1016/j.scitotenv.2020.143861>, 2021.
- 715 Bakker, D. C., Pfeil, B., Landa, C. S., Metzl, N., O'Brien, K. M., Olsen, A., Smith, K., Cosca, C., Harasawa, S., and Jones, S. D.: A multi-decade record of high-quality fCO<sub>2</sub> data in version 3 of the Surface Ocean CO<sub>2</sub> Atlas (SOCAT), *Earth System Science Data*, 8, 383, <https://doi.org/10.5194/essd-8-383-2016>, 2016.
- Bates, N., and Mathis, J.: The Arctic Ocean marine carbon cycle: evaluation of air-sea CO<sub>2</sub> exchanges, ocean acidification impacts and potential feedbacks, *Biogeosciences*, 6, 2433-2459, doi:10.5194/bg-6-2433-2009, 2009.
- 720 Brown, K. A., Williams, W. J., Carmack, E. C., Fiske, G., François, R., McLennan, D., and Peucker-Ehrenbrink, B.: Geochemistry of small Canadian Arctic Rivers with diverse geological and hydrological settings, *Journal of Geophysical Research: Biogeosciences*, 125, e2019JG005414, 2020.
- Butterworth, B. J., and Else, B. G.: Dried, closed-path eddy covariance method for measuring carbon dioxide flux over sea ice, *Atmospheric Measurement Techniques*, 11, 6075-6090, <https://doi.org/10.5194/amt-11-6075-2018>, 2018.
- 725 Butterworth, B. J., Else, B. G., Brown, K. A., Mundy, C. J., Rotermund, L. M., William, W. J., and Boer, G. d.: Annual carbon dioxide flux over seasonal sea ice in the Canadian Arctic, In prep, 2022.
- Cai, W.-J., Chen, L., Chen, B., Gao, Z., Lee, S. H., Chen, J., Pierrot, D., Sullivan, K., Wang, Y., and Hu, X.: Decrease in the CO<sub>2</sub> uptake capacity in an ice-free Arctic Ocean basin, *Science*, 329, 556-559, DOI: 10.1126/science.1189338, 2010.
- 730 Chierici, M., Fransson, A., Lansard, B., Miller, L. A., Mucci, A., Shadwick, E., Thomas, H., Tremblay, J., and Papakyriakou, T. N.: Impact of biogeochemical processes and environmental factors on the calcium carbonate saturation state in the Circumpolar Flaw Lead in the Amundsen Gulf, Arctic Ocean, *Journal of Geophysical Research: Oceans*, 116, <https://doi.org/10.1029/2011JC007184>, 2011.
- Cruz-García, R., Ortega, P., Guemas, V., Acosta Navarro, J. C., Massonnet, F., and Doblas-Reyes, F. J.: An anatomy of Arctic sea ice forecast biases in the seasonal prediction system with EC-Earth, *Climate Dynamics*, 56, 1799-1813, <https://doi.org/10.1007/s00382-020-05560-4>, 2021.
- 735 Dalman, L. A., Else, B. G., Barber, D., Carmack, E., Williams, W. J., Campbell, K., Duke, P. J., Kirillov, S., Mundy, C. J., and Tremblay, J.-É.: Enhanced bottom-ice algal biomass across a tidal strait in the Kitikmeot Sea of the Canadian Arctic, *Elementa: Science of the Anthropocene*, 7, <https://doi.org/10.1525/elementa.361>, 2019.
- 740 DeGrandpre, M., Evans, W., Timmermans, M. L., Krishfield, R., Williams, B., and Steele, M.: Changes in the Arctic Ocean carbon cycle with diminishing ice cover, *Geophysical research letters*, 47, e2020GL088051, <https://doi.org/10.1002/essoar.10502603.1>, 2020.
- Dickson, A. G., and Millero, F. J.: A comparison of the equilibrium constants for the dissociation of carbonic acid in seawater media, *Deep Sea Research Part A. Oceanographic Research Papers*, 34, 1733-1743, [https://doi.org/10.1016/0198-0149\(87\)90021-5](https://doi.org/10.1016/0198-0149(87)90021-5), 1987.
- 745 Dickson, A. G.: Thermodynamics of the dissociation of boric acid in synthetic seawater from 273.15 to 318.15 K, *Deep Sea Research Part A. Oceanographic Research Papers*, 37, 755-766, 1990.
- Dickson, A. G., Sabine, C. L., and Christian, J. R.: Guide to best practices for ocean CO<sub>2</sub> measurements, North Pacific Marine Science Organization, Sidney, British Columbia, 191, 2007.
- 750 Dong, Y., Yang, M., Bakker, D. C., Kitidis, V., and Bell, T. G.: Uncertainties in eddy covariance air-sea CO<sub>2</sub> flux measurements and implications for gas transfer velocity parameterisations, *Atmospheric Chemistry and Physics*, 21, 8089-8110, 2021a.
- Dong, Y., Yang, M., Bakker, D. C., Liss, P. S., Kitidis, V., Brown, I., Chierici, M., Fransson, A., and Bell, T. G.: Near-Surface Stratification Due to Ice Melt Biases Arctic Air-Sea CO<sub>2</sub> Flux Estimates, *Geophysical research letters*, 48, e2021GL095266, <https://doi.org/10.1029/2021GL095266>, 2021b.
- 755 Duke, P., Else, B., Jones, S., Marriot, S., Ahmed, M., Nandan, V., Butterworth, B., Gonski, S., Dewey, R., and Sastri, A.: Seasonal marine carbon system processes in an Arctic coastal landfast sea ice environment observed with an innovative underwater sensor platform, *Elementa: Science of the Anthropocene*, 9, 00103, <https://doi.org/10.1525/elementa.2021.00103>, 2021.
- 760 Else, B., Galley, R., Papakyriakou, T., Miller, L., Mucci, A., and Barber, D.: Sea surface pCO<sub>2</sub> cycles and CO<sub>2</sub> fluxes at landfast sea ice edges in Amundsen Gulf, Canada, *Journal of Geophysical Research: Oceans*, 117, <https://doi.org/10.1029/2012JC007901>, 2012.

- Else, B. G., Whitehead, J. J., Galindo, V., Ferland, J., Mundy, C., Gonski, S. F., Ehn, J. K., Rysgaard, S., and Babin, M.: Response of the Arctic marine inorganic carbon system to ice algae and under-ice phytoplankton blooms: A case study along the fast-ice edge of Baffin Bay, *Journal of Geophysical Research: Oceans*, 124, 1277-1293, <https://doi.org/10.1029/2018JC013899>, 2019.
- 765 Else, B. G., Cranch, A., Sims, R. P., Jones, S., Dalman, L. A., Mundy, C. J., Segal, R. A., Scharien, R. K., and Guha, T.: Variability in sea ice carbonate chemistry: a case study comparing the importance of ikaite precipitation, bottom-ice algae, and currents across an invisible polynya, *The Cryosphere*, 16, 3685-3701, 2022.
- 770 Evans, W., Pocock, K., Hare, A., Weekes, C., Hales, B., Jackson, J., Gurney-Smith, H., Mathis, J. T., Alin, S. R., and Feely, R. A.: Marine CO<sub>2</sub> patterns in the northern salish sea, *Frontiers in Marine Science*, 5, 536, <https://doi.org/10.3389/fmars.2018.00536>, 2019.
- Ford, J. D., Smit, B., Wandel, J., Allurut, M., Shappa, K., Ittusarjuat, H., and Qrunnut, K.: Climate change in the Arctic: current and future vulnerability in two Inuit communities in Canada, *Geographical Journal*, 174, 45-62, <https://doi.org/10.1111/j.1475-4959.2007.00249.x>, 2008.
- 775 Geilfus, N.-X., Galley, R., Crabeck, O., Papakyriakou, T., Landy, J., Tison, J.-L., and Rysgaard, S.: Inorganic carbon dynamics of melt-pond-covered first-year sea ice in the Canadian Arctic, *Biogeosciences*, 12, 2047-2061, <https://doi.org/10.5194/bg-12-2047-2015>, 2015.
- 780 Geilfus, N.-X., Pind, M., Else, B., Galley, R., Miller, L., Thomas, H., Gosselin, M., Rysgaard, S., Wang, F., and Papakyriakou, T.: Spatial and temporal variability of seawater pCO<sub>2</sub> within the Canadian Arctic Archipelago and Baffin Bay during the summer and autumn 2011, *Continental Shelf Research*, 156, 1-10, 2018.
- Harris, L. N., Yurkowski, D. J., Gilbert, M. J., Else, B. G., Duke, P. J., Ahmed, M. M., Tallman, R. F., Fisk, A. T., and Moore, J.: Depth and temperature preference of anadromous Arctic char *Salvelinus alpinus* in the Kitikmeot Sea, a shallow and low-salinity area of the Canadian Arctic, *Marine Ecology Progress Series*, 634, 175-197, <https://doi.org/10.3354/meps13195>, 2020.
- 785 Ho, D. T., and Schanze, J. J.: Precipitation-Induced Reduction in Surface Ocean pCO<sub>2</sub>: Observations From the Eastern Tropical Pacific Ocean, *Geophysical research letters*, 47, e2020GL088252, <https://doi.org/10.1029/2020GL088252>, 2020.
- Jakobsson, M.: Hypsometry and volume of the Arctic Ocean and its constituent seas, *Geochemistry, Geophysics, Geosystems*, 3, 1-18, 2002.
- 790 JCGM: Evaluation of measurement data—Guide to the expression of uncertainty in measurement, 134, 2008.
- Kalnay, E., Kanamitsu, M., Kistler, R., Collins, W., Deaven, D., Gandin, L., Iredell, M., Saha, S., White, G., and Woollen, J.: The NCEP/NCAR 40-year reanalysis project, *Bulletin of the American Meteorological Society*, 77, 437-472, [https://doi.org/10.1175/1520-0477\(1996\)077<0437:TNYRP>2.0.CO;2](https://doi.org/10.1175/1520-0477(1996)077<0437:TNYRP>2.0.CO;2), 1996.
- 795 Kim, K., Ha, S.-Y., Kim, B. K., Mundy, C., Gough, K. M., Pogorzelec, N. M., and Lee, S. H.: Carbon and nitrogen uptake rates and macromolecular compositions of bottom-ice algae and phytoplankton at Cambridge Bay in Dease Strait, Canada, *Annals of Glaciology*, 61, 106-116, <https://doi.org/10.1017/aog.2020.17>, 2020.
- Kljun, N., Calanca, P., Rotach, M., and Schmid, H. P.: A simple two-dimensional parameterisation for Flux Footprint Prediction (FFP), *Geoscientific Model Development*, 8, 3695-3713, 2015.
- 800 Landrum, L., and Holland, M. M.: Extremes become routine in an emerging new Arctic, *Nature Climate Change*, 10, 1108-1115, <https://doi.org/10.1038/s41558-020-0892-z>, 2020.
- Landschützer, P., Laruelle, G. G., Roobaert, A., and Regnier, P.: A uniform pCO<sub>2</sub> climatology combining open and coastal oceans, *Earth System Science Data*, 12, 2537-2553, <https://doi.org/10.5194/essd-12-2537-2020>, 2020.
- 805 Lewis, E., Wallace, D., and Allison, L. J.: Program developed for CO<sub>2</sub> system calculations, Carbon Dioxide Information Analysis Center, managed by Lockheed Martin Energy Research Corporation for the US Department of Energy Tennessee, 1998.
- Loose, B., Schlosser, P., Perovich, D., Ringelberg, D., Ho, D., Takahashi, T., Richter-Menge, J., Reynolds, C., McGillis, W., and Tison, J.-L.: Gas diffusion through columnar laboratory sea ice: implications for mixed-layer ventilation of CO<sub>2</sub> in the seasonal ice zone, *Tellus B: Chemical and Physical Meteorology*, 63, 23-39, <https://doi.org/10.1111/j.1600-0889.2010.00506.x>, 2011.
- 810



- Macdonald, R., Anderson, L., Christensen, J., Miller, L., Semiletov, I., and Stein, R.: The Arctic Ocean: budgets and fluxes, in: Carbon and Nutrient Fluxes in Continental Margins: A Global Synthesis, , edited by: Liu, K., Atkinson, , L., Q., and R., T.-M., Springer-Verlag, Berlin Heidelberg, 291–303, 2010.
- 815 Manning, C. C., Preston, V. L., Jones, S. F., Michel, A. P., Nicholson, D. P., Duke, P. J., Ahmed, M. M., Manganini, K., Else, B. G., and Tortell, P. D.: River inflow dominates methane emissions in an Arctic coastal system, *Geophysical research letters*, 47, e2020GL087669, <https://doi.org/10.1029/2020GL087669>, 2020.
- Martin, J., Dumont, D., and Tremblay, J. É.: Contribution of subsurface chlorophyll maxima to primary production in the coastal Beaufort Sea (Canadian Arctic): A model assessment, *Journal of Geophysical Research: Oceans*, 118, 5873–5886, <https://doi.org/10.1002/2013JC008843>, 2013.
- 820 Mehrbach, C., Culberson, C. H., Hawley, J. E., and Ptkowicz, R. M.: Measurement of the apparent dissociation constants of carbonic acid in seawater at atmospheric pressure, *Limnol. Oceanogr.*, 897–907, 1973.
- Meire, L., Sogaard, D., Mortensen, J., Meysman, F., Soetaert, K., Arendt, K., Juul-Pedersen, T., Blicher, M., and Rysgaard, S.: Glacial meltwater and primary production are drivers of strong CO<sub>2</sub> uptake in fjord and coastal waters adjacent to the Greenland Ice Sheet, *Biogeosciences*, 12, 2347–2363, 2015.
- 825 Miller, L. A., Burgers, T. M., Burt, W. J., Granskog, M. A., and Papakyriakou, T. N.: Air-Sea CO<sub>2</sub> Flux Estimates in Stratified Arctic Coastal Waters: How Wrong Can We Be?, *Geophysical research letters*, 46, 235–243, <https://doi.org/10.1029/2018GL080099>, 2018.
- Mundy, C., Gosselin, M., Ehn, J., Gratton, Y., Rossnagel, A., Barber, D. G., Martin, J., Tremblay, J. É., Palmer, M., and Arrigo, K. R.: Contribution of under-ice primary production to an ice-edge upwelling phytoplankton bloom in the Canadian Beaufort Sea, *Geophysical research letters*, 36, <https://doi.org/10.1029/2009GL038837>, 2009.
- 830 Nightingale, P. D., Malin, G., Law, C. S., Watson, A. J., Liss, P. S., Liddicoat, M. I., Boutin, J., and Upstill-Goddard, R. C.: In situ evaluation of air-sea gas exchange parameterizations using novel conservative and volatile tracers, *Global Biogeochemical Cycles*, 14, 373–387, <https://doi.org/10.1029/1999GB900091>, 2000.
- Parmentier, F.-J. W., Christensen, T. R., Sørensen, L. L., Rysgaard, S., McGuire, A. D., Miller, P. A., and Walker, D. A.: 835 The impact of lower sea-ice extent on Arctic greenhouse-gas exchange, *Nature Climate Change*, 3, 195–202, <https://doi.org/10.1038/nclimate1784>, 2013.
- Perrette, M., Yool, A., Quartly, G., and Popova, E. E.: Near-ubiquity of ice-edge blooms in the Arctic, *Biogeosciences*, 8, 515–524, <https://doi.org/10.5194/bg-8-515-2011>, 2011.
- Peterson, J. T., Komhyr, W., Waterman, L., Gammon, R., Thoning, K., and Conway, T.: Atmospheric CO<sub>2</sub> variations at Barrow, Alaska, 1973–1982, in: Scientific Application of Baseline Observations of Atmospheric Composition (SABOAC), edited by: Ehhalt, D., Pearman, G., and Galbally, I., Springer, Dordrecht, 397–416, 1987.
- 840 Sims, R. P., Schuster, U., Watson, A. J., Yang, M. X., Hopkins, F. E., Stephens, J., and Bell, T. G.: A measurement system for vertical seawater profiles close to the air–sea interface, *Ocean Science*, 13, 649–660, <https://doi.org/10.5194/os-13-649-2017>, 2017.
- 845 Spreen, G., Kaleschke, L., and Heygster, G.: Sea ice remote sensing using AMSR-E 89-GHz channels, *Journal of Geophysical Research: Oceans*, 113, <https://doi.org/10.1029/2005JC003384>, 2008.
- Takahashi, T., Olafsson, J., Goddard, J. G., Chipman, D. W., and Sutherland, S.: Seasonal variation of CO<sub>2</sub> and nutrients in the high-latitude surface oceans: A comparative study, *Global Biogeochemical Cycles*, 7, 843–878, <https://doi.org/10.1029/93GB02263>, 1993.
- 850 Teodoru, C. R., Del Giorgio, P. A., Prairie, Y. T., and Camire, M.: Patterns in pCO<sub>2</sub> in boreal streams and rivers of northern Quebec, Canada, *Global Biogeochemical Cycles*, 23, <https://doi.org/10.1029/2008GB003404>, 2009.
- Van Heuven, S., Pierrot, D., Rae, J., Lewis, E., and Wallace, D.: MATLAB Program Developed for CO<sub>2</sub> System Calculations. ORNL/CDIAC-105b. Carbon Dioxide Information Analysis Center, Oak Ridge National Laboratory, US Department of Energy, Oak Ridge, Tennessee, [cdiac.ornl.gov/ftp/co2sys/CO2SYS\\_calc\\_MATLAB\\_v1](http://cdiac.ornl.gov/ftp/co2sys/CO2SYS_calc_MATLAB_v1), 1, 1, 2011.
- 855 Wang, Q., Myers, P. G., Hu, X., and Bush, A. B.: Flow constraints on pathways through the Canadian Arctic Archipelago, *Atmosphere-Ocean*, 50, 373–385, <https://doi.org/10.1080/07055900.2012.704348>, 2012.
- Wanninkhof, R.: Relationship between wind speed and gas exchange over the ocean revisited, *Limnology and Oceanography: Methods*, 12, 351–362, <https://doi.org/10.4319/lom.2014.12.351>, 2014.
- 860 Weiss, R. F.: Carbon dioxide in water and seawater: the solubility of a non-ideal gas, *Marine chemistry*, 2, 203–215, [http://dx.doi.org/10.1016/0304-4203\(74\)90015-2](http://dx.doi.org/10.1016/0304-4203(74)90015-2), 1974.

- Wessel, P., and Smith, W. H.: A global, self-consistent, hierarchical, high-resolution shoreline database, *Journal of Geophysical Research: Solid Earth*, 101, 8741-8743, <https://doi.org/10.1029/96JB00104>, 1996.
- Williams, W., Brown, K. A., Bluhm, B., Carmack, E. C., Dalman, L., Danielson, S. L., Else, B. G., Friedriksen, R., Mundy, C., and Rotermund, L. M.: Stratification in the Canadian Arctic Archipelago's Kitikmeot Sea: biological and geochemical consequences, *Polar Knowledge Canada*, Ottawa, Canada, 46-52, 2018.
- 865 Woolf, D. K., Shutler, J. D., Goddijn-Murphy, L., Watson, A., Chapron, B., Nightingale, P. D., Donlon, C. J., Piskozub, J., Yelland, M., and Ashton, I.: Key uncertainties in the recent air-sea flux of CO<sub>2</sub>, *Global Biogeochemical Cycles*, 33, 1548-1563, <https://doi.org/10.1029/2018GB006041>, 2019.
- 870 Wynja, V., Demers, A.-M., Laforest, S., Lacelle, M., Pasher, J., Duffe, J., Chaudhary, B., Wang, H., and Giles, T.: Mapping coastal information across Canada's northern regions based on low-altitude helicopter videography in support of environmental emergency preparedness efforts, *Journal of Coastal Research*, 31, 276-290, <https://doi.org/10.2112/JCOASTRES-D-14-00059.1>, 2015.
- 875 Xu, C., Mikhael, W., Myers, P. G., Else, B., Sims, R. P., and Zhou, Q.: Effects of Seasonal Ice Coverage on the Physical Oceanographic Conditions of the Kitikmeot Sea in the Canadian Arctic Archipelago, *Atmosphere-Ocean*, 59, 1-19, <https://doi.org/10.1080/07055900.2021.1965531>, 2021.